NOAA Technical Memorandum ERL ESG-2

MULTI-SCALE ANALYSES OF METEOROLOGICAL CONDITIONS AFFECTING PAN AMERICAN WORLD AIRWAYS FLIGHT 759

F. Caracena
R. A. Maddox

Weather Research Program
Boulder, Colorado

J. F. W. Purdom
J. F. Weaver
R. N. Green

National Environmental Data Information and Satellite Service
Regional and Mesoscale Meteorology Branch
Ft. Collins, Colorado

Environmental Sciences Group
Boulder, Colorado
January 1983

UNITED STATES DEPARTMENT OF COMMERCE
Malcolm Baldrige, Secretary

NATIONAL OCEANIC AND ATMOSPHERIC ADMINISTRATION
John V. Byrne, Administrator

Environmental Research Laboratories
George H. Ludwig Director

NOTICE

Mention of a commercial company or product does not constitute an endorsement by NOAA Environmental Research Laboratories. Use for publicity or advertising purposes of information from this publication concerning proprietary products or the tests of such products is not authorized.

CONTENTS

1. INTRODUCTION

On the afternoon of July 9th, 1982, Pan American World Airways Flight 759, a Boeing 727 aircraft, crashed in Kenner, Louisiana, shortly after taking off from New Orleans International Airport (Moisant Field). The airplane crashed into a residential area of Kenner, approximately three quarters of a mile off the departure end of runway 10 (i.e. heading 100^{o} degrees) at about 4:10 p.m. Central Daylight Time (CDT), or 2110 Greenwich Mean Time (GMT). Many residences were either destroyed or damaged in the crash. The accident killed 145 persons on the aircraft and 8 persons on the ground. At the time of Flight 759's departure there were thunderstorms in the New Orleans area. In addition, while the plane was taxiing to the takeoff runway, personnel in the New Orleans tower issued several wind shear advisories for winds that had activated the airport's low-level windshear alert warning system. Therefore, it was not surprising that speculations immediately arose about the weather, and low-level windshear in particular, being a cause of the accident. Indeed, much of the testimony during the National Transportation Safety Board's (NTSB) September fact finding hearings centered around the weather conditions and their possible effects upon the aircraft.

The seriousness of this particular event provided the motivation for a detailed examination of the meteorological conditions at the time of the accident. The goal was to reconstruct the evolution of weather events immediately before and during the crash so that the precise role of meteorological features could be assessed by the NTSB Board of Inquiry. The meteorological analyses discussed in this report range from brief descriptions of the large-scale weather patterns---utilizing routinely available NWS weather charts---down to very detailed reconstructions of small-scale features at the time of the crash. Since the small-scale analysis effort relied heavily upon the accounts of witnesses, there is necessarily a degree of uncertainty present that cannot be

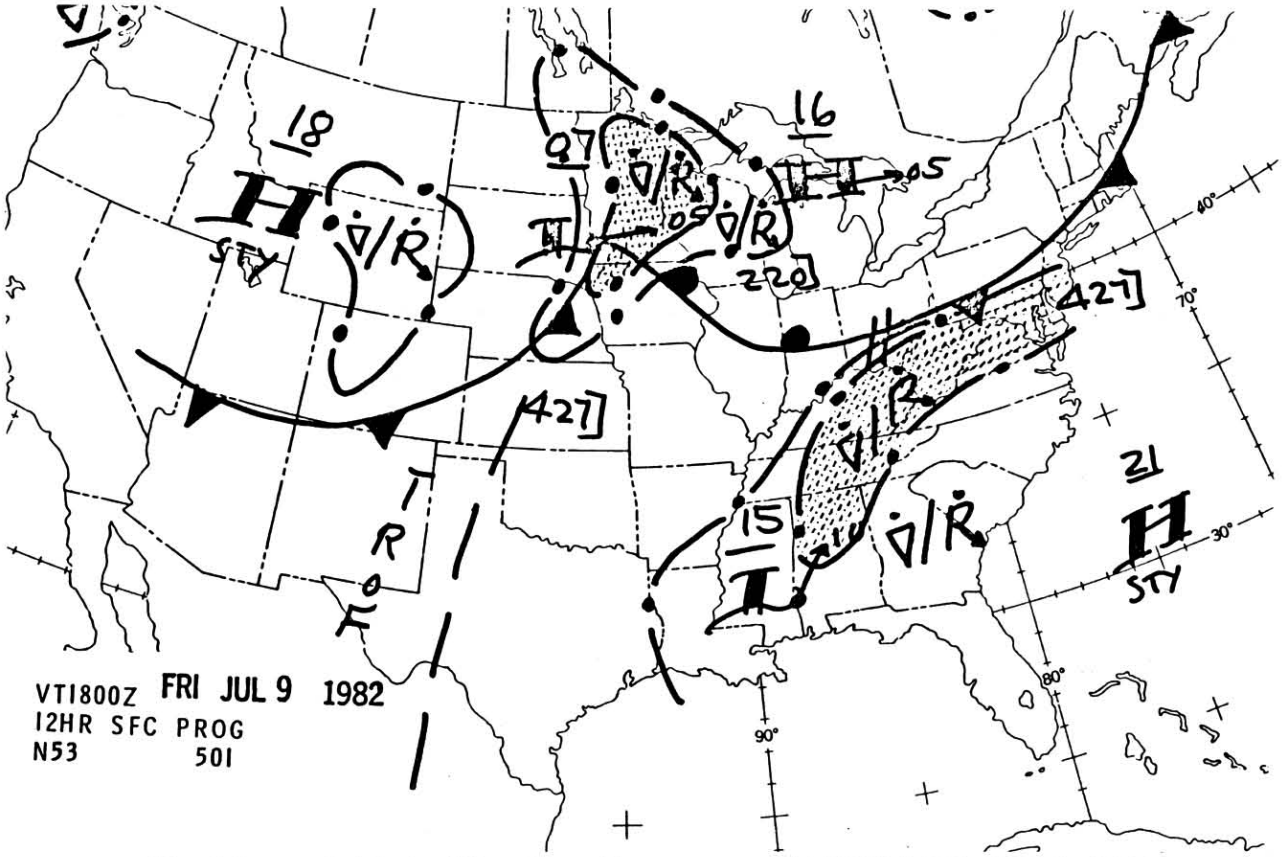

Fig. 2.1 NWS significant weather prog. valid 1800 GMT, 09 July 1982.

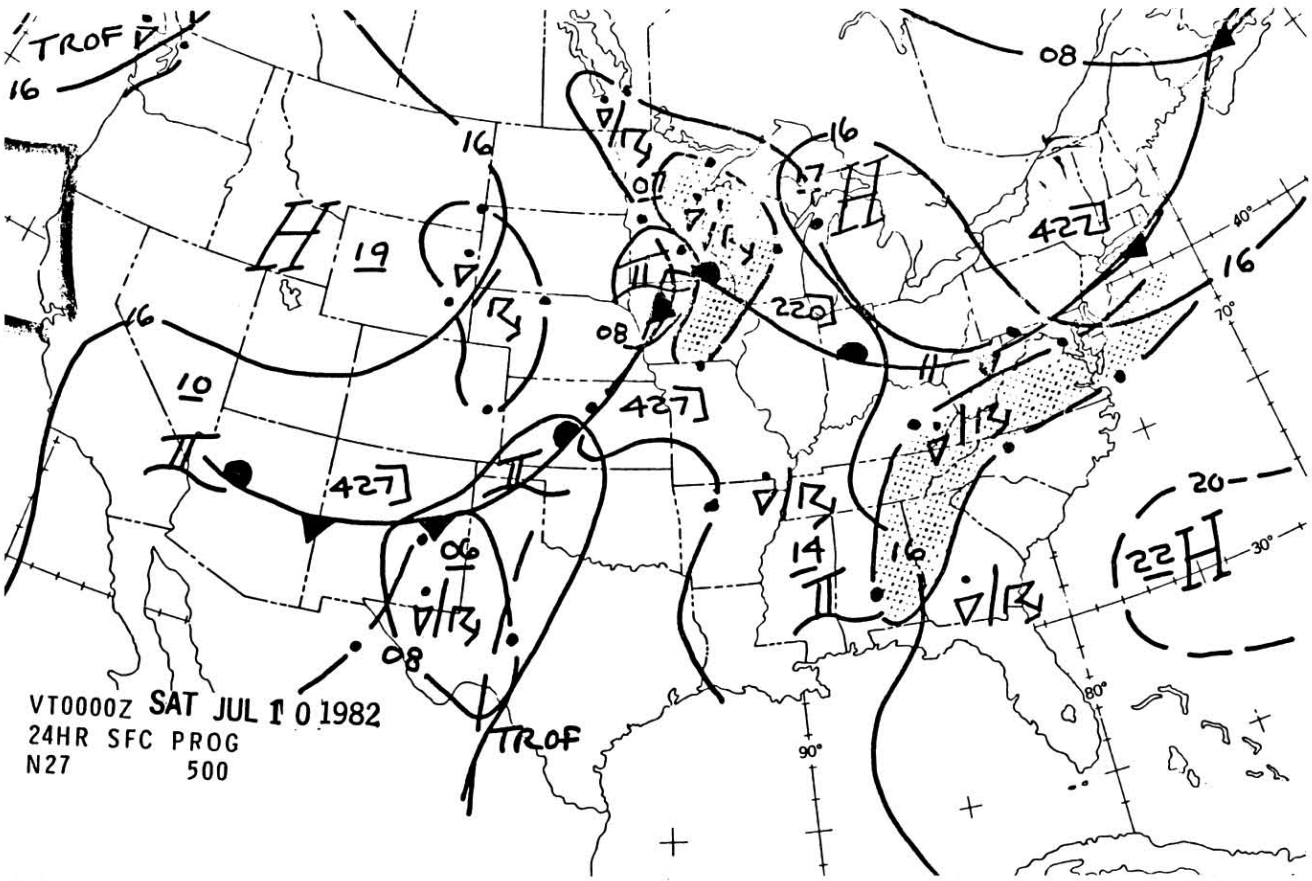

Fig. 2.2 NWS significant weather prog. valid 0000 GMT, 10 July 1982.

quantified. Similarly, the analyses of local conditions are very complex and we cannot claim that our solutions are unique. However, we do feel that our solutions are meteorologically sound and consistent with both the accounts of eyewitnesses and quantitative information from the aircraft's flight recorder.

2. LARGE-SCALE METEOROLOGICAL PATTERNS

Conditions along the central Gulf coast on the afternoon of July 9th can be characterized as generally typical of summertime in the southeastern United States. Widespread air mass thunderstorms occurred, as forecast, within a subtropical high pressure area. There were no fronts or intense large-scale low pressure centers within more than 1000 km of Louisiana, so meteorological features were generally quite weak.

The NWS surface prognoses valid at 1800 GMT on the 9th and 0000 GMT on July 10th are shown in Figs. 2.1 and 2.2. These charts illustrate the synoptic scale situation and the forecast of widespread afternoon shower and thunderstorm activity across the southeastern U.S. Note that a very weak (central pressure ~ 1014 mb) surface low pressure area was moving slowly across Mississippi during this period. The NWS afternoon analyses (surface chart for 2100 GMT - Fig. 2.3; radar summary chart for 2035 GMT-Fig.2.4; and ceiling/visibility chart for 2200 GMT - Fig. 2.5) show that conditions evolved essentially as indicated both in the charts shown in Figs. 2.1 and 2.2 and the NWS terminal forecast for Moisant Field (MSY), which called for scattered, variable to broken, clouds at 3000 ft. with a chance for 1000 ft. overcast and 2 miles visibility in moderate thunderstorms after 1700 GMT. Note in Fig. 2.4 that the only severe thunderstorm watch in effect was over Iowa, far removed from the region of the plane crash. The radar summary chart did indicate a number of slowly moving, heavy thunderstorms (tops from 47,000 to 57,000 feet MSL) over the central Gulf coast region. Again, this represents a fairly typical summertime situation.

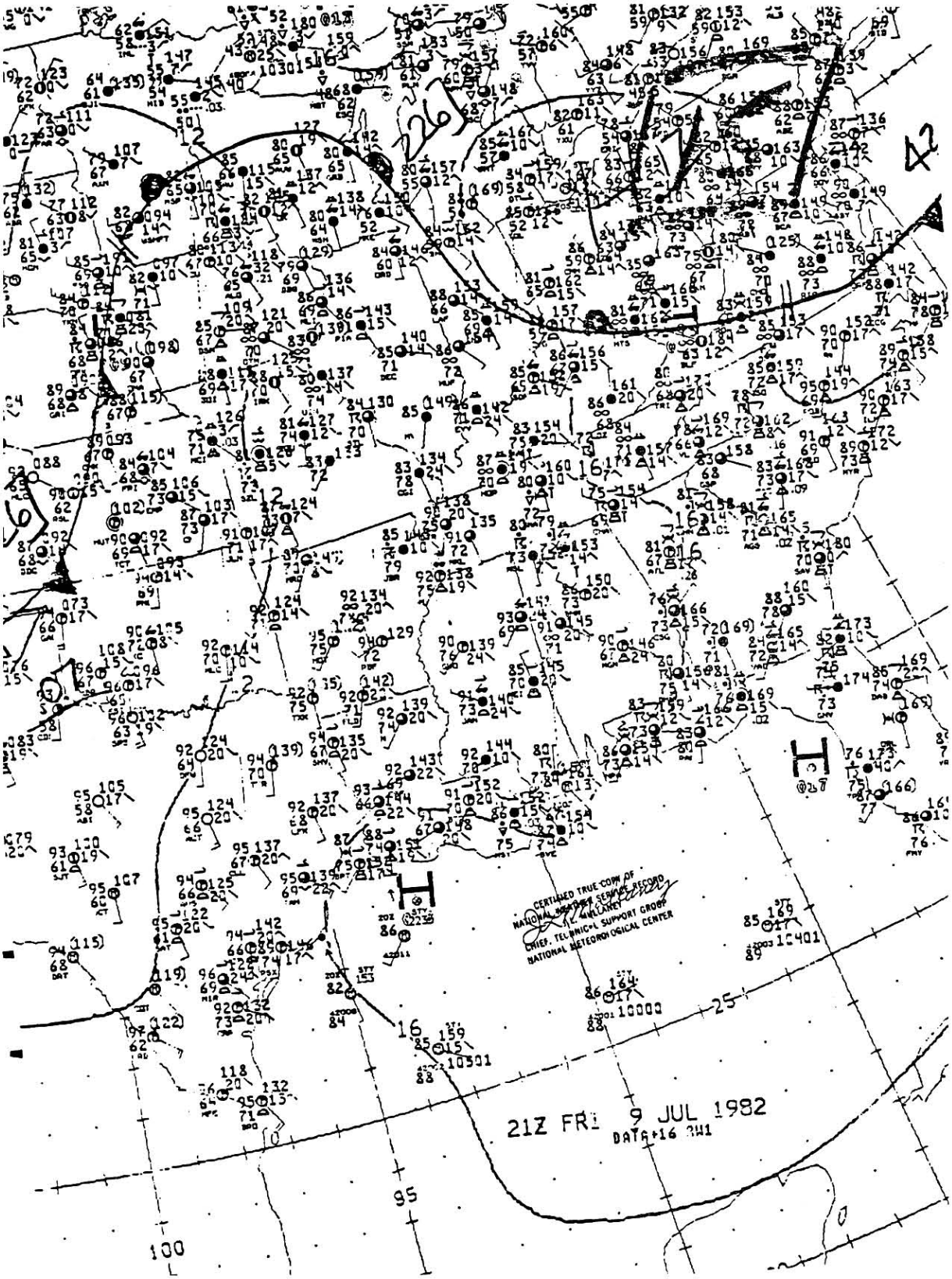

Fig. 2.3 NWS surface analysis for 2100 GMT, 09 July 1982.

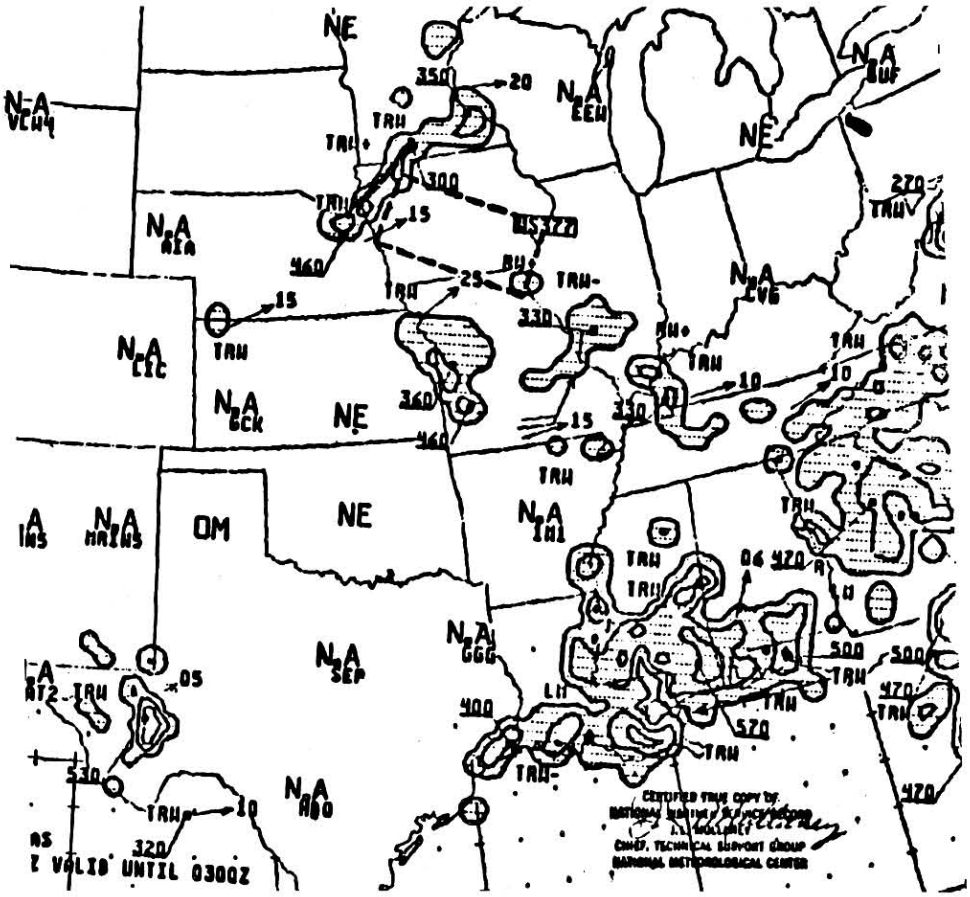

Fig. 2.4 NWS radar summary chart for 2035 GMT, 09 July 1982.

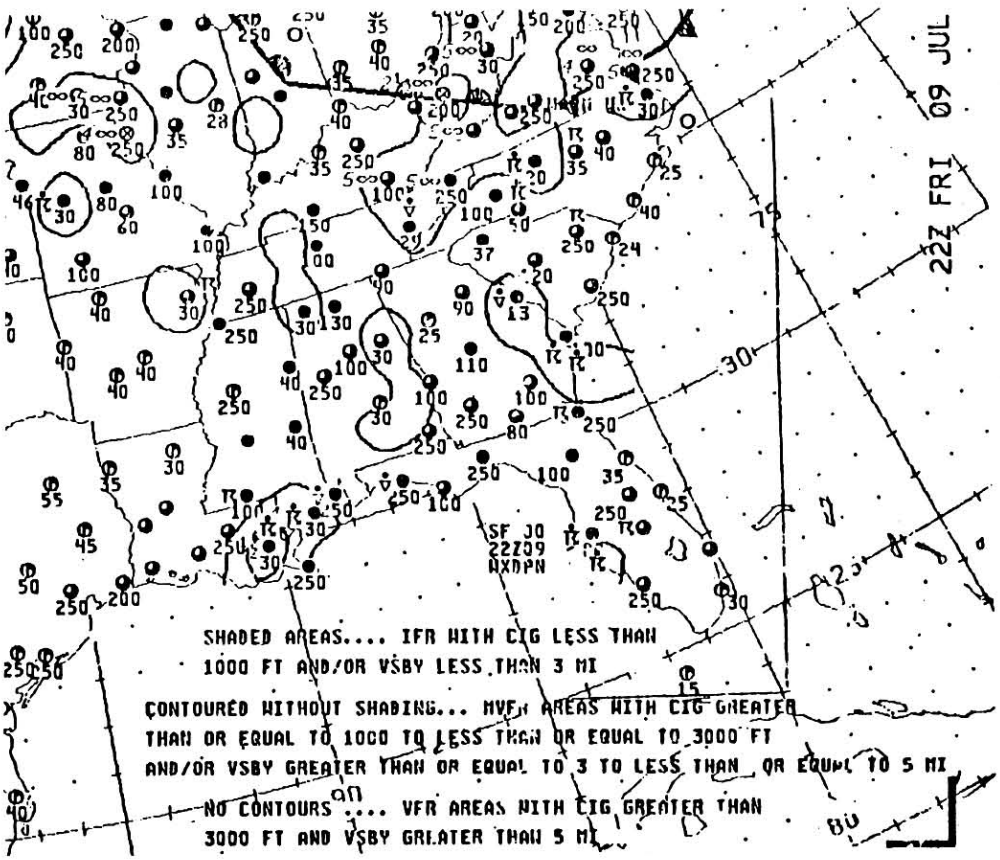

Fig. 2.5 NWS ceiling and visibility analysis for 2200 GMT, 09 July 1982.

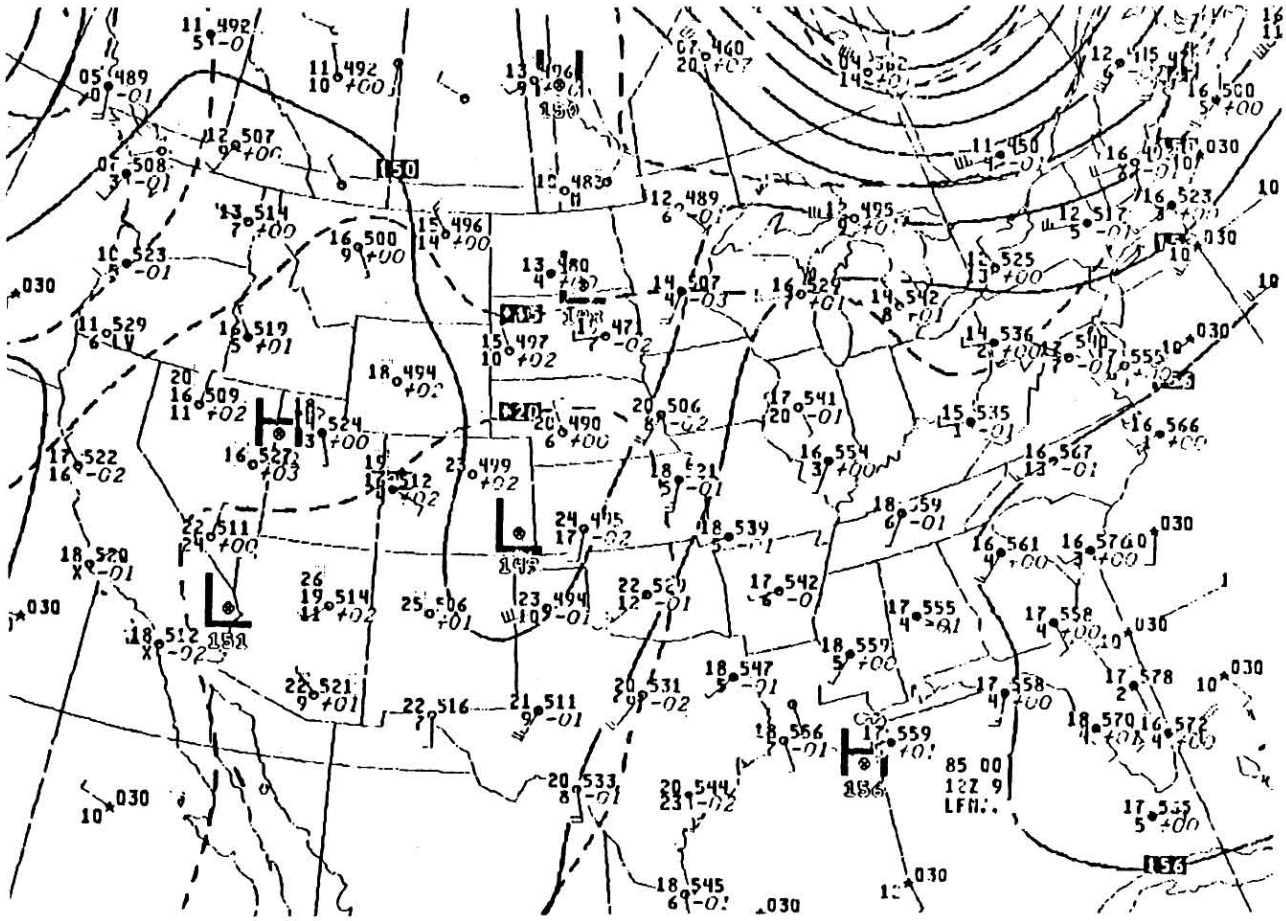

Fig. 2.6 NWS 850 mb analysis for 1200 GMT, 09 July 1982.

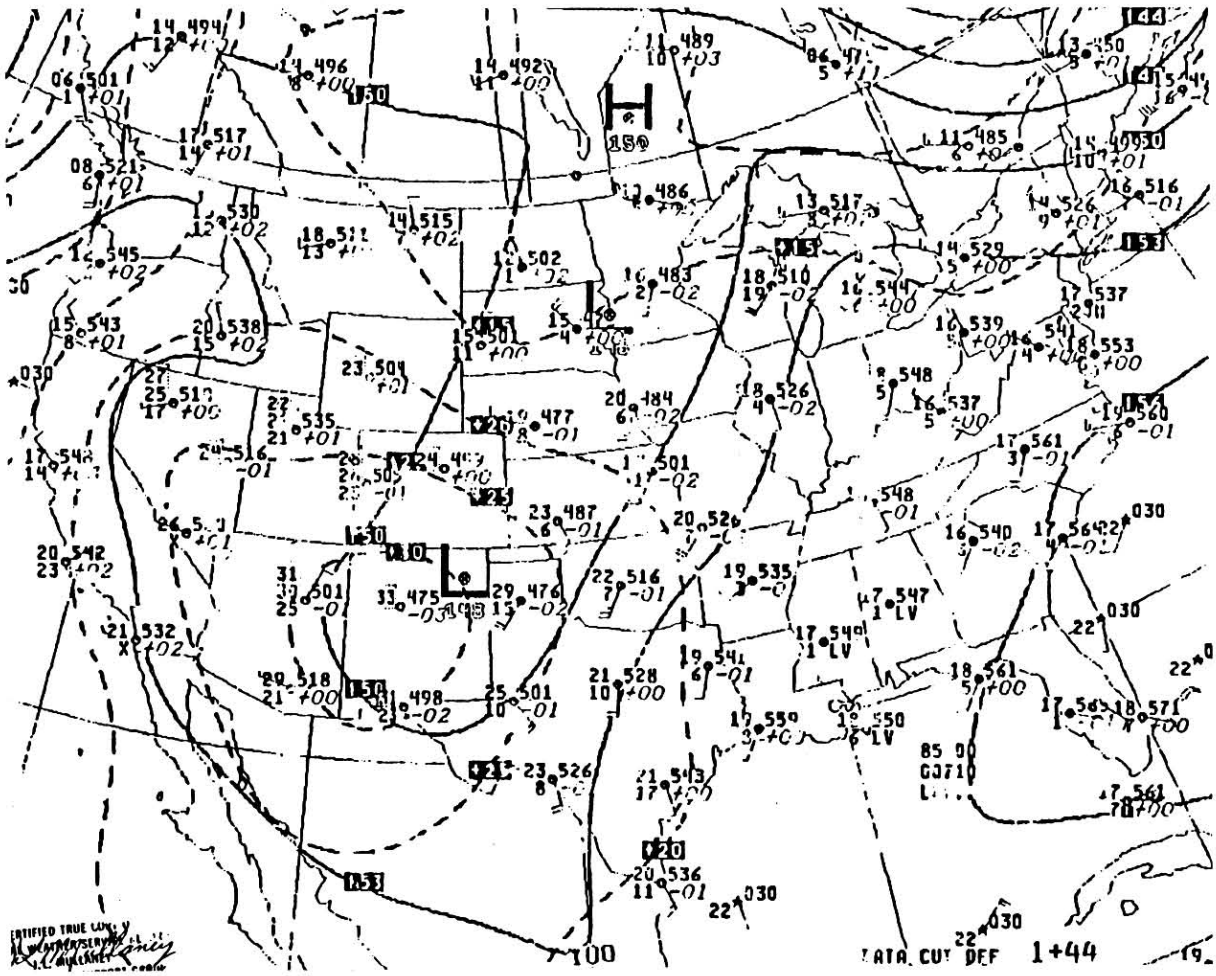

Fig. 2.7 NWS 850 mb analysis for 0000 GMT, 10 July 1982.

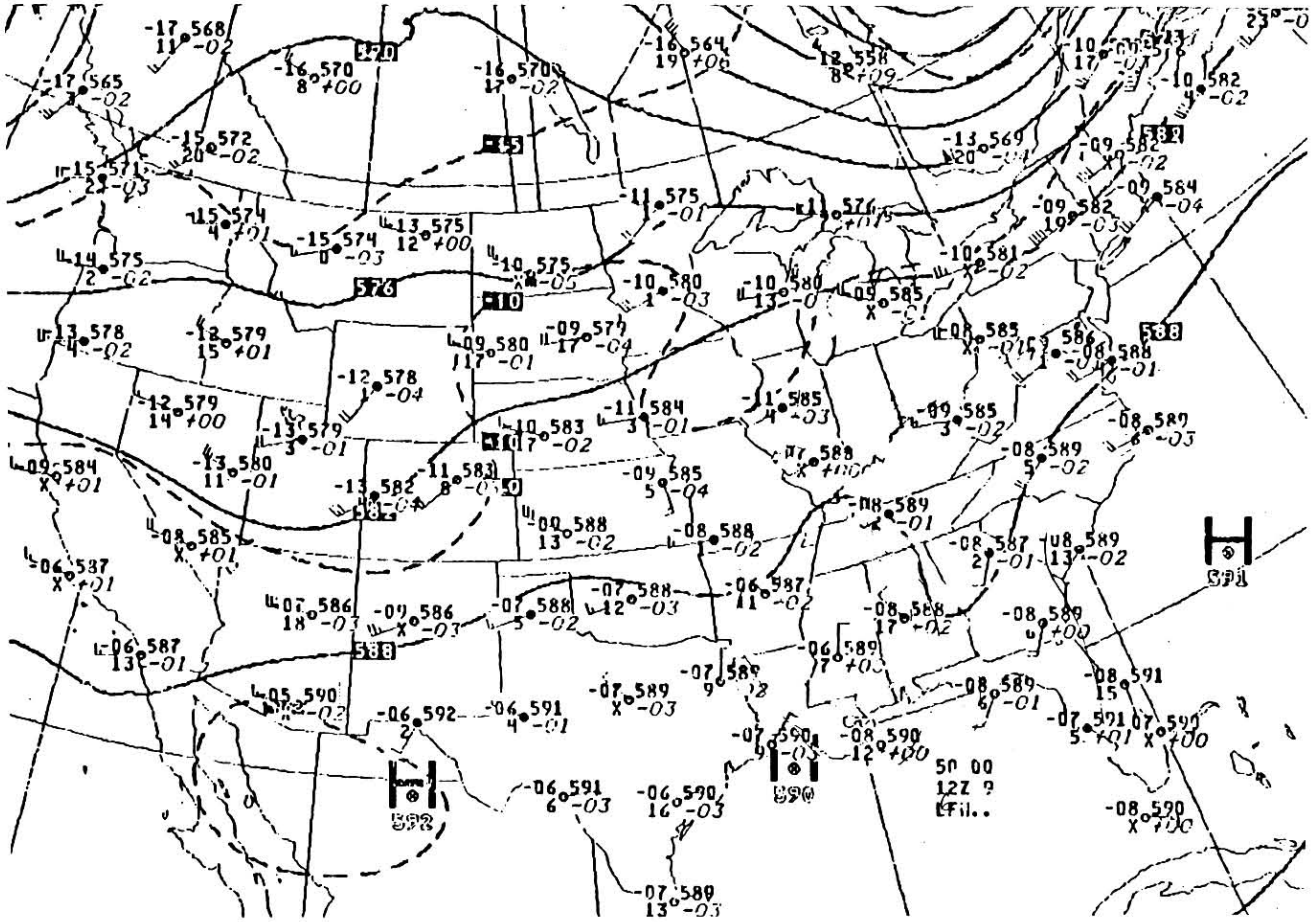

Fig. 2.8 NWS 500 mb analysis for 1200 GMT, 09 July 1982.

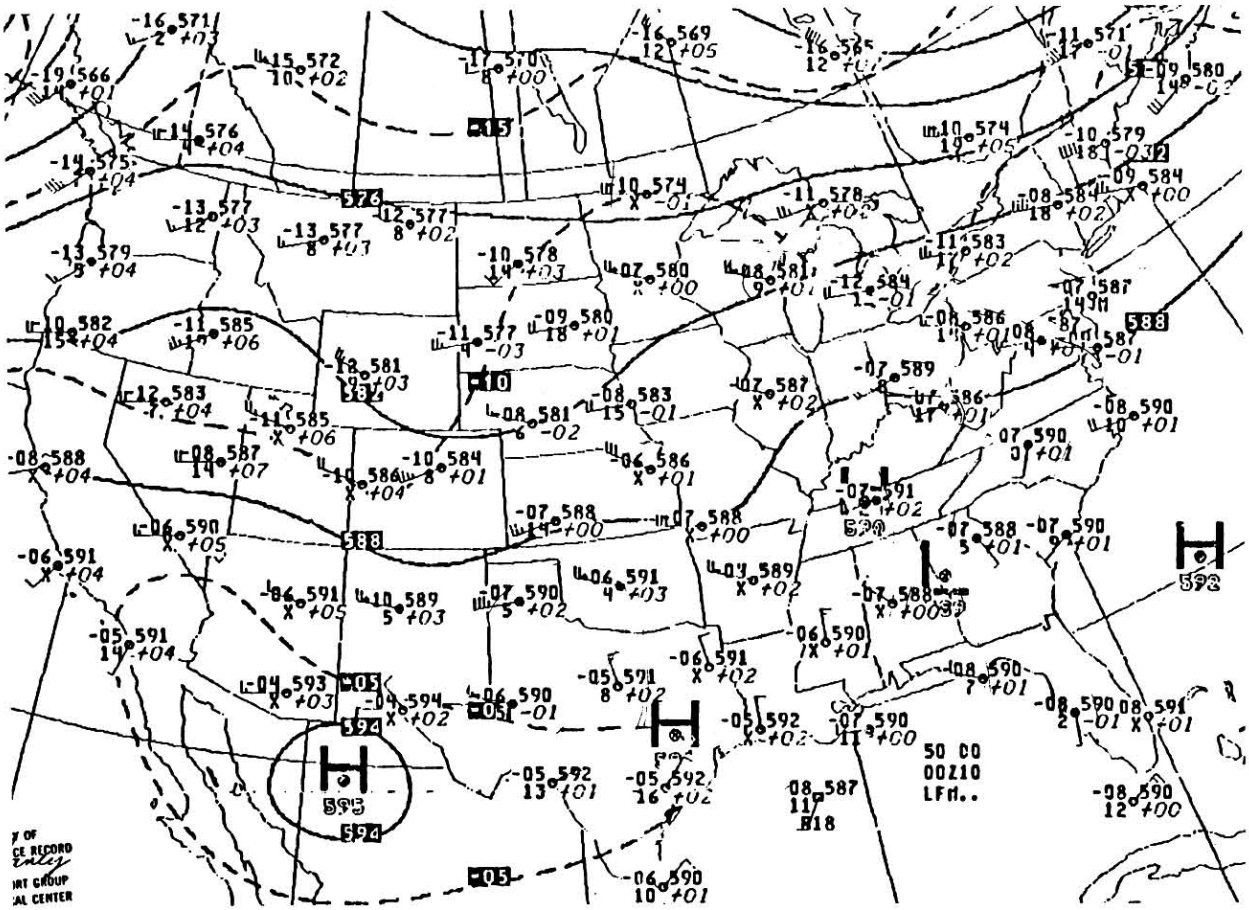

Fig. 2.9 NWS 500 mb analysis for 0000 GMT, 10 July 1982.

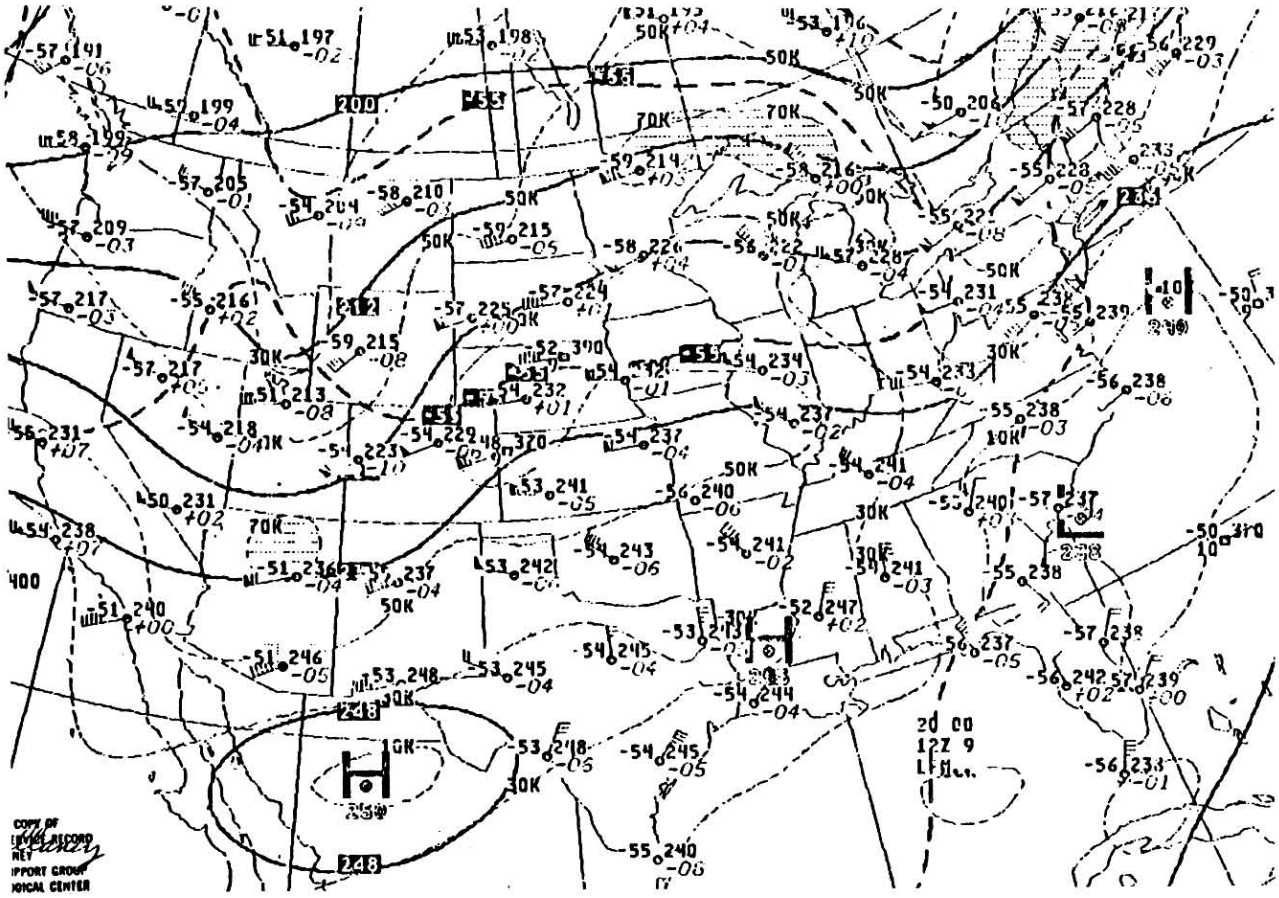

Fig. 2.10 NWS 200 mb analysis for 1200 GMT, 09 July 1982.

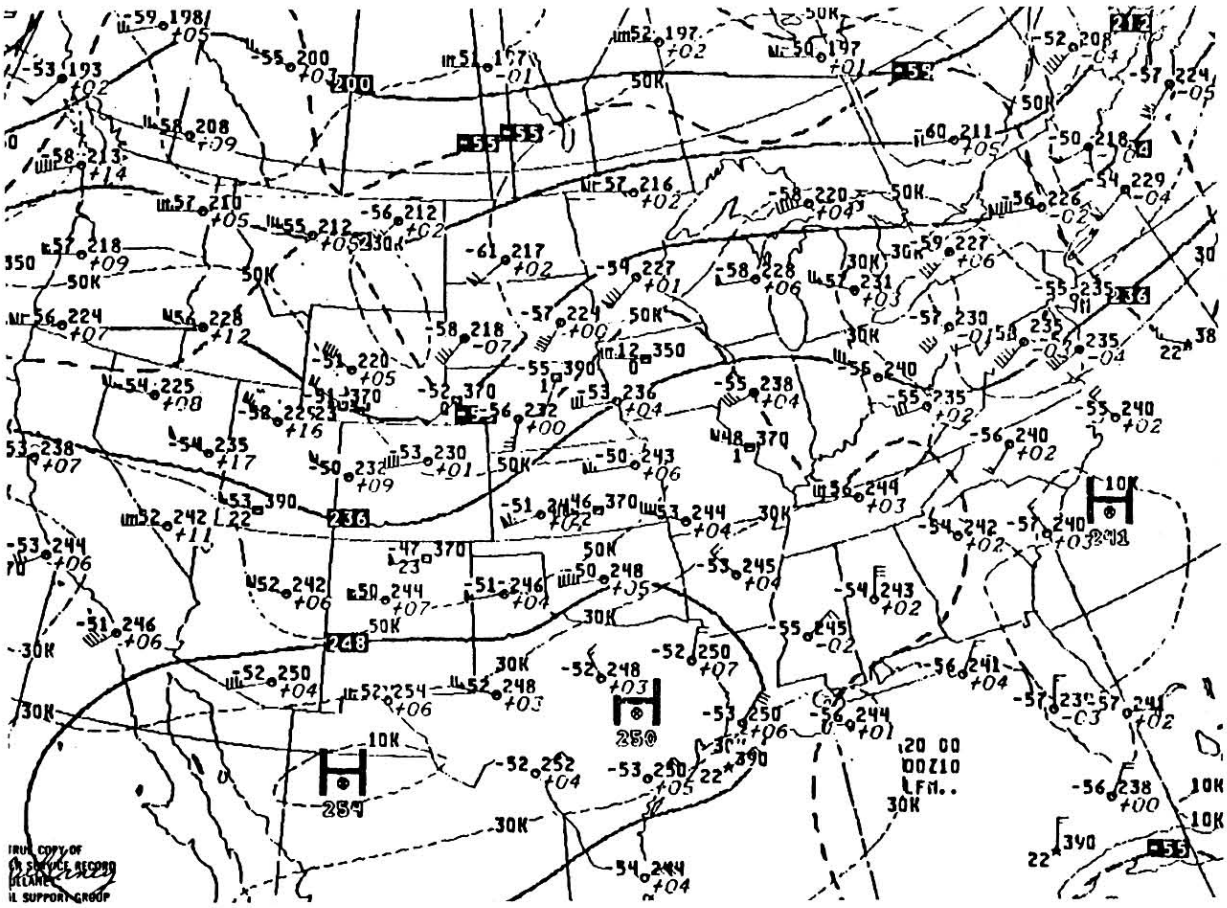

Fig. 2.11 NWS 200 mb analysis for 0000 GMT, 10 July 1982.

The NWS analysis charts for 850, 500 and 200 mb, at both 1200 GMT (9 hours prior to the crash) and 0000 GMT (shortly after the accident), are shown in Figs. 2.6 through 2.11. These analyses indicate that lower levels in the troposphere (i.e. 850 mb) were characterized by light and variable winds and high moisture contents across the central Gulf region. In mid-levels (i.e. 500 mb), flow was northerly and light (generally less than 15 kts). Pronounced drying did occur in mid-levels during the day on the 9th, especially over Arkansas, Louisana and Mississippi. Upper-level (i.e. 200 mb) analyses exhibited relatively light (generally less than 30 kts) northerly flow. Indeed, this map series might best be characterized by the innocuous nature of the large-scale meteorological setting.

A more detailed analysis of surface conditions over the southeast U.S. for 2100 GMT is shown in Fig. 2.12. This analysis indicates that, even though large-scale systems were lacking, there were a number of mesoscale (i.e. on the order of 200 to 500 km lengths) convective outflows and pressure perturbations present. The mesohighs and regions of thunderstorm activity corresponded well with clearly defined, convectively produced, pockets of cooler air. Even these smaller-scale surface features (not routinely analyzed in NWS operations) were located primarily to the east and northeast of the New Orleans local area. A very detailed analysis of conditions in mid-levels (500 mb--shown in Fig. 2.13) depicts the presence of a very weak trough aloft over the Southeast. The trailing end of this trough was located near the New Orleans area at the time of the accident. Its primary role in the afternoon's events was probably in helping to trigger shower and thunderstorm activity over the region. There is one feature of specific interest shown on the map. A large pocket of very dry (indicated by the "X" temperature-dewpoint depressions), potentially cool air developed (probably due to subsidence to the rear of the weak short wave) over the lower Mississippi Valley during the course of the day. This dry mid-level air was positioned so that it might be entrained

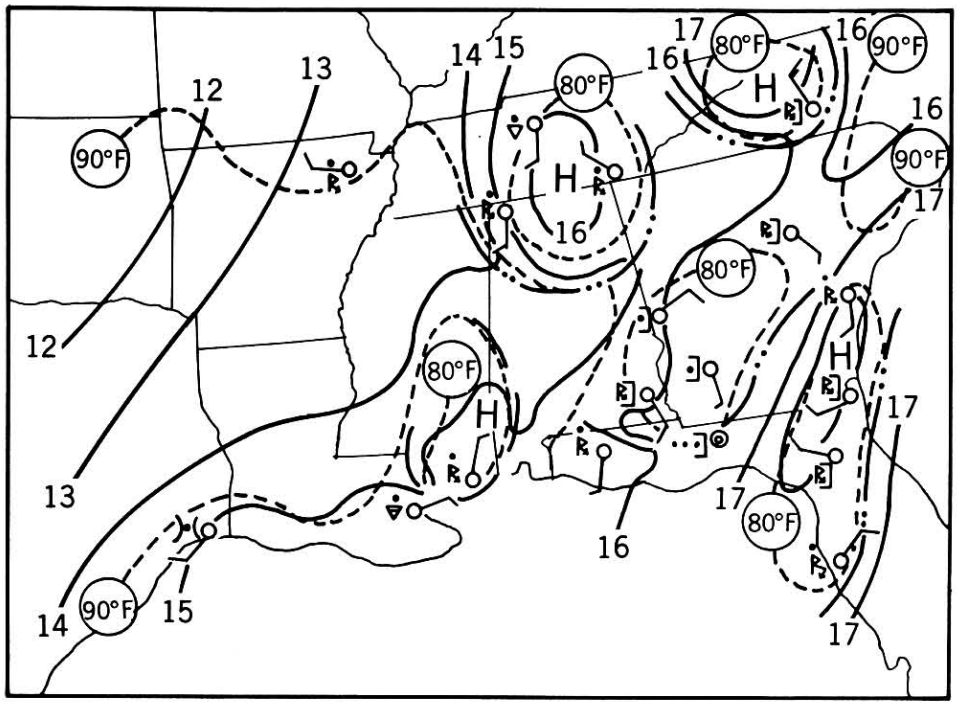

Fig. 2.12 Detailed surface analysis for 2100 G M T, 09 July 1982.

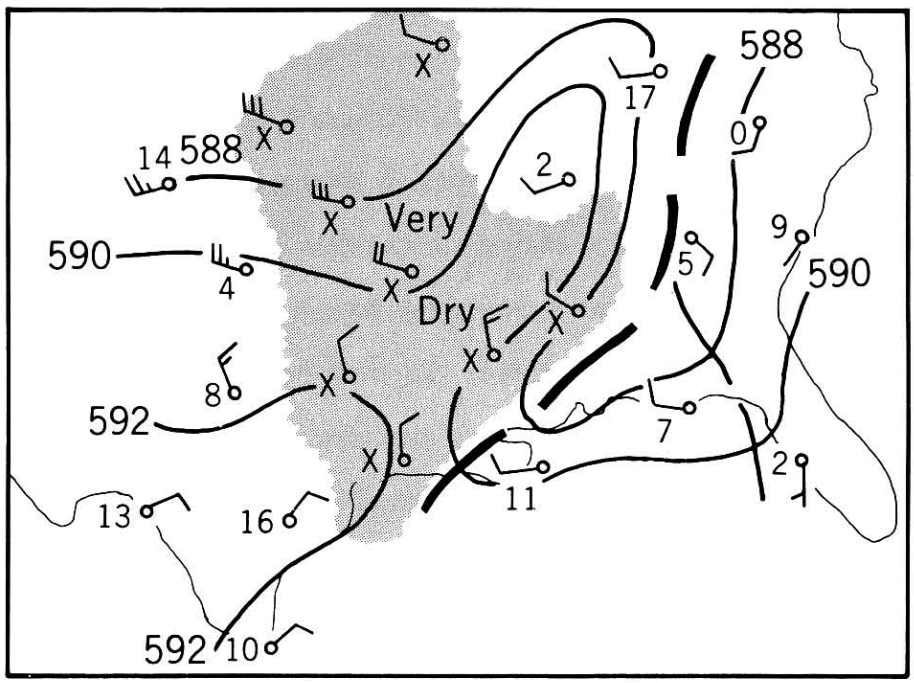

Fig. 2.13 Detailed 500 mb analysis for 0000 G M T, 10 July 1982.

into thunderstorms over the lower-Mississippi Valley. Entrainment of this dry air would be conducive to development of stronger thunderstorm downdrafts than might be expected were the air mass distinctly moist throughout the troposphere.

3. SATELLITE ANALYSES

The discussion in this Section is based on GOES-West, visual and infrared data. July 9, 1982, was a 3-minute interval imaging (RRSD) day, thus post-processing has allowed a more detailed look at this case than is normally possible (i.e., with the normal 30 minute interval data). Additionally, the interactive imaging system at Colorado State University (see Green and Kruidenier, 1982, for details) was available to help make precise cloud top temperature measurements and to construct movie loops from the 3-minute interval, visible and infrared data. Movie loops are particularly helpful in identifying small-scale weather features that may not be notable on individual photographs. The development of organized cloud patterns is often associated with small-scale features that are readily detectable in an animated loop, while the rest of the cloud field forms, moves and dissipates in a less organized fashion around them. It should be mentioned that neither RRSD data nor movie loops are available to forecasters in real time.

Often the air in one region has different pressure, temperature or moisture characteristics (and thus may have a different density) than that in another. These differences are important factors in atmospheric dynamics, since inclement weather often occurs at boundaries separating air masses. One common example is a cold front. Other examples include:

i) Sea breezes - formed due to the difference in heating rates between land and adjacent water (e.g., Haurwitz, 1947);

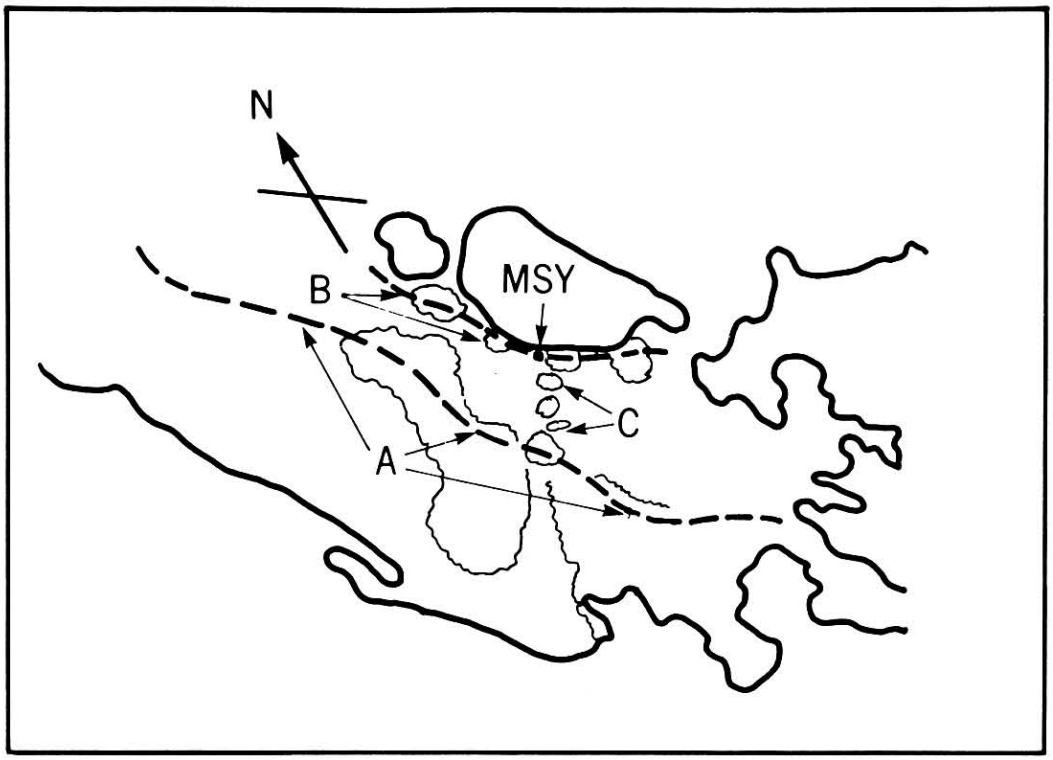

Fig. 3.1 a) Visible satellite imagery from GOES-WEST at 2005 GMT, and b) important boundaries at the same time. Boundary A is a sea breeze, B a lake breeze, and C is a convective line.

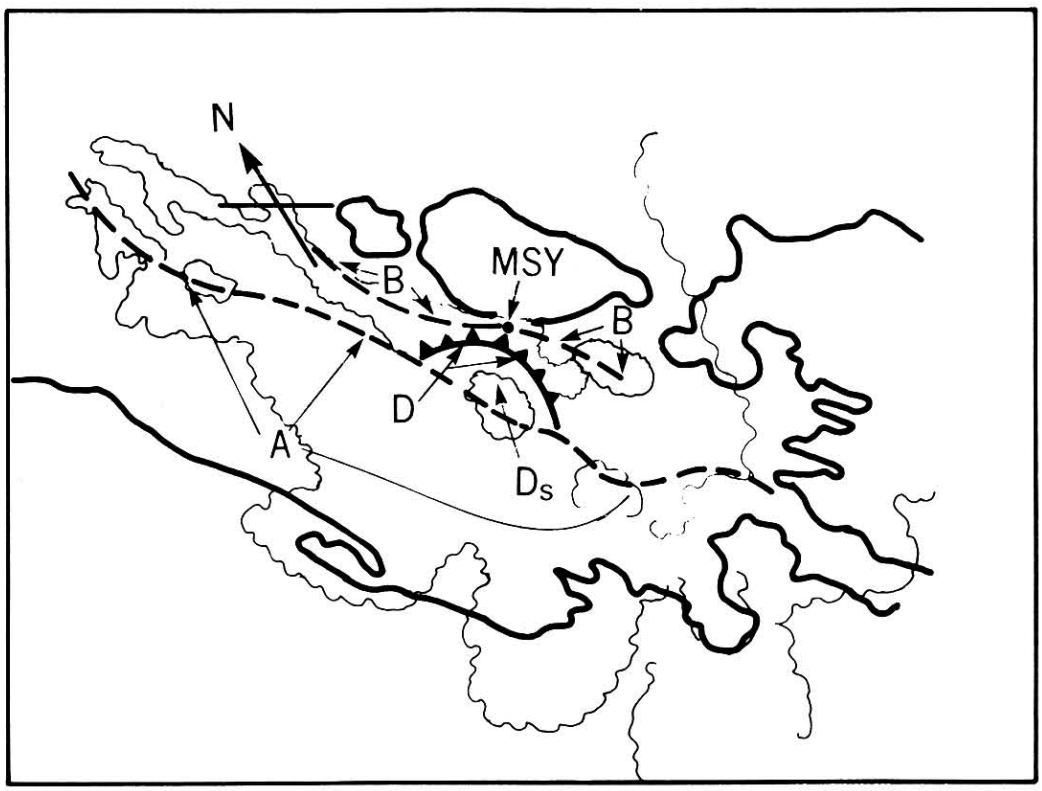

Fig. 3.2 Same as Fig. 4.1 for 2045 GMT. Boundary D is a thunderstorm outflow boundary which originated with storm D_s.

ii) Lake breezes - as in sea breezes (e.g., Chandik and Lyons, 1971);

iii) Thunderstorm outflows - formed by rain-cooled air as it spreads out and away from thunderstorms (e.g., Purdom, 1976).

Such boundaries are commonly identifiable on satellite imagery as organized cloud lines. Not only do such lines often mark the location of subsequent storm development (Purdom, 1976), but many times the most intense activity becomes fixed to these boundaries (Weaver, 1979).

Detailed study of RRSD satellite imagery (refer to Appendix B for definitions of common satellite terminology) from the July 9th case revealed several low-level boundaries in the vicinity of MSY (Figs. 3.1 and 3.2). These included:

i) A sea breeze that moved northward from the Gulf coast a ~ 12 kts (Feature A, Fig. 3.1);

ii) A lake breeze which remained nearly stationary throughout most of the afternoon (B, Fig. 3.1);

iii) A convective line that formed along a boundary separating what had earlier in the day been a stratus and fog covered region to its west and a clear area to its east (C, Fig. 3.1); and

iv) A thunderstorm outflow boundary (D, Fig. 3.2) associated with the storm labeled D_S.

TABLE 3.1 Storm growth rates at MSY.

Time	Brightness Temp (°C)	Height (KFT) From 00Z LCH Sounding	ΔH/Δt FPM	MPS
2101	-11.7	21.3		
			>966	4.8
2104	-17.2	24.2		
			>1600	8.0
2107	-28.0	29.0		
			>1033	5.2
2110	-36.2	32.1		
			> 700	3.5
2113	-41.2	34.2		

Our interpretation of the satellite data places the intersection point of the lake breeze with boundary C over Moisant Field. The sea breeze is moving into that area from the south and thunderstorm outflow D in (Fig. 3.2) is moving rapidly northward (~23 kts) toward MSY.

As noted in Appendix B, the size of an IR Pixel is greater than 4.0 x 2.0 miles for U.S. latitudes. In fact, at $30^{o}N/90^{o}W$, the resolution for GOES-W is approximately 7.0 x 4.0 miles, owing to the earth's curvature. This means that one IR Pixel represents the average radiated temperature from an area considerably larger than the size of the entire airport. Analysis of radar data (Sect. 4.1) and precipitation patterns (Sect. 4.2) shows that the activity within a single IR pixel over the airport was actually composed of a number of individual cells. However, one can reach certain conclusions by looking at the growth rates of the convective activity over the airport versus rates nearby. (Note that the IR cloud top temperature can be related to height in the atmosphere and temperature change can then be related to vertical cloud growth.)

Tables 3.1 and 3.2 make such comparisons. In table 3.2 the "nearby area" represents several small storm areas monitored over southern Louisiana. The general indication of these data is that other storm areas were growing at roughly half the rate as that over the airport at the time of the accident. The activity on 9 July would most likely have gone unnoticed if the intersection had not occurred directly over a high traffic air facility, and been the site of an aircraft accident. In cases such as July 9, 1982, the routine detection of such intersections would require 1) Rapid-Scan data, 2) real-time availability of these data, and 3) equipment for analyzing the data (e.g., animated looping capability, temperature extraction capability, etc.). The means to detect these intersections, on a real-time basis, are not available to operational forecasters.

Table 3.2 Storm growth rates, nearby region.

Time (GMT)	Brightness Temp (°C)	Height (KFT) From 00Z LCH Sounding	ΔH/Δt FPM	ΔH/Δt MPS
2101	-26.2	28.0		
			>667	3.3
2104	-30.7	30.0		
			>500	2.5
2107	-34.2	31.5		
			>667	3.3
2110	-39.2	33.5		
			>333	3.3
2113	-42.2	34.5		

4.0 SMALL SCALE ANALYSES

4.1 Radar Data

A series of photographs of the Slidell radar (an NWS WSR-57, 10-cm wavelength radar) scope were carefully analyzed. The Slidell radar is located about 30 miles east-northeast of MSY. The radar echoes and analyses shown and discussed in this Section were developed using highly enlarged projections of film loops of the radar scope photographs. Because the echoes located near MSY were at the edge of the ground clutter pattern, special care was taken to identify and track evolving precipitation echoes accurately. Ambiguities were resolved by looping the radar film forward and back in time repeatedly. Accurate spatial positioning of the echoes was made possible by radar returns from a signigicant landmark - the Lake Pontchartrain Causeway.

The Slidell scope photographs, reproduced in Figs. 4.1-4.5, are in reasonably close agreement with the satellite-based interpretations. The sea breeze front apparently extended eastward along an arc from a line of Video Integrator Processor (VIP) level 4 echoes just southwest of Lake Salvador. (Note that VIP level 2, 3 and 4 echoes are categorized as moderate, strong and very strong and correspond to rainfall rates of 0.2 to 1.1, 1.1 to 2.2 and 2.2 to 4.5 in/h respectively.) Two VIP level 4 echoes located east of New Orleans developed along the eastern end of the lake breeze front. The thermal boundary that extended south from MSY is marked (in Fig. 4.1) by a cluster of echoes along the west shore of Lake Salavador. From 2048 to 2114 GMT the lake breeze front and the thermal boundary remained nearly stationary while the sea breeze front advanced toward MSY. As the sea breeze front approached, a VIP level 2 echo over MSY intensified to VIP level 3 by 2058 GMT (Fig. 4.2). This level 3 echo lingered over the

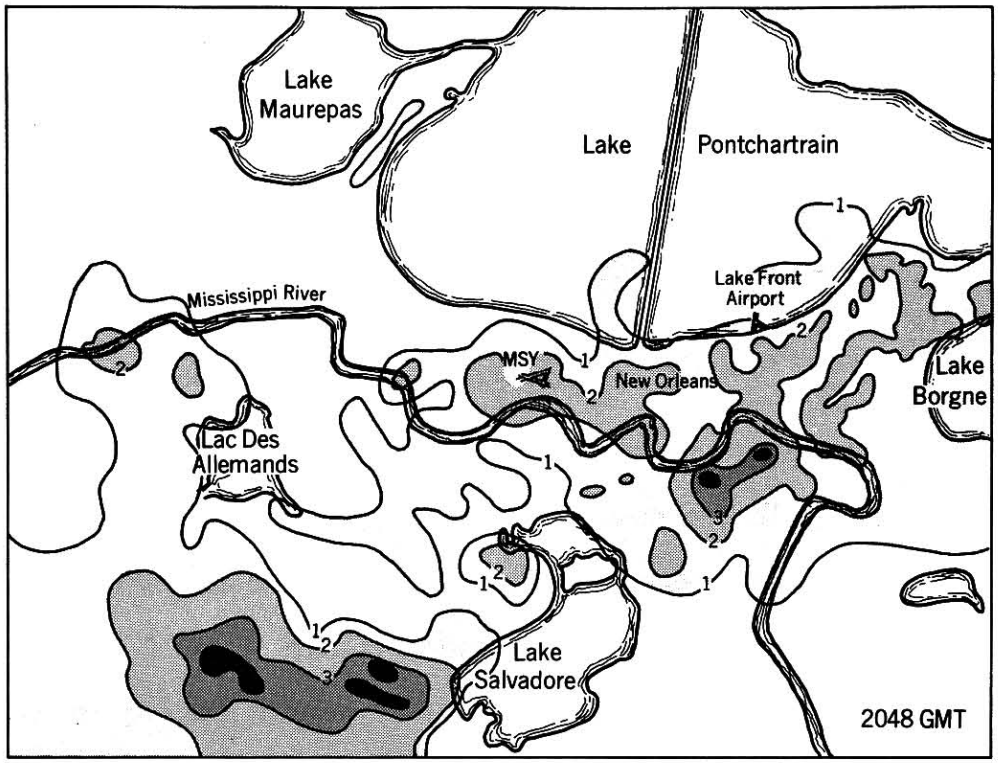

Fig. 4.1 The first of a time series of Slidell radar echoes beginning with this figure at 2048 GMT, 09 July 1982. The gray shades represent VIP levels 1,2, and 3 with the darker shades representing the higher level. Areas of VIP level 4 or greater are shaded black.

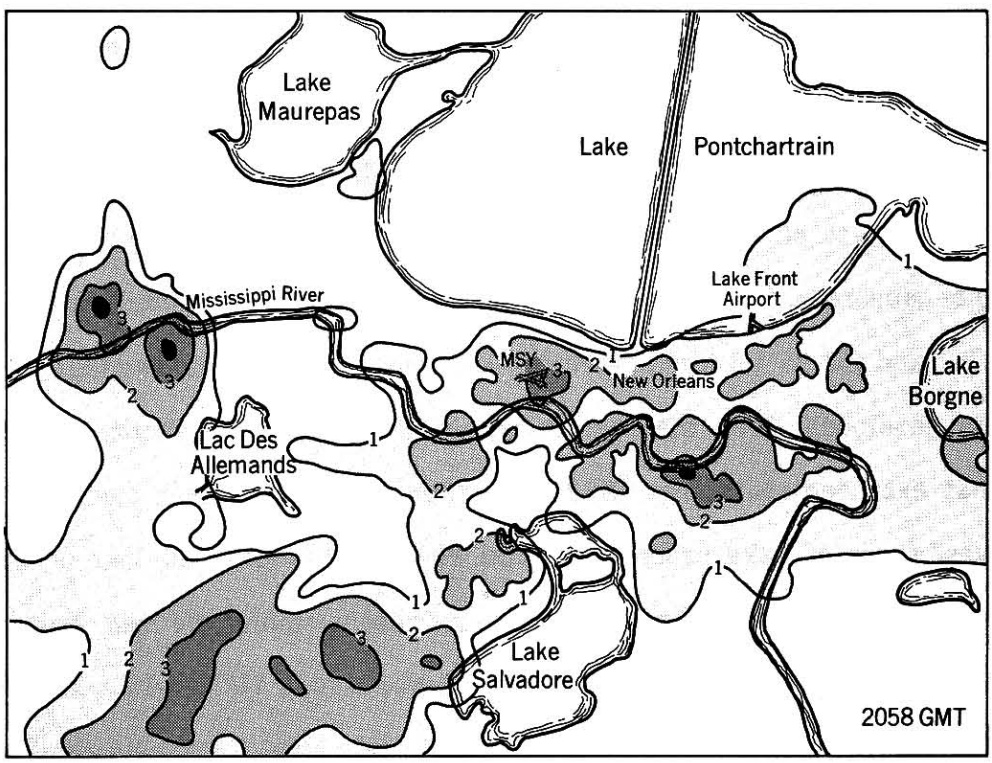

Fig. 4.2 Slidell radar plot for 2058 GMT, 09 July 1982. See Fig. 3.1 caption for details.

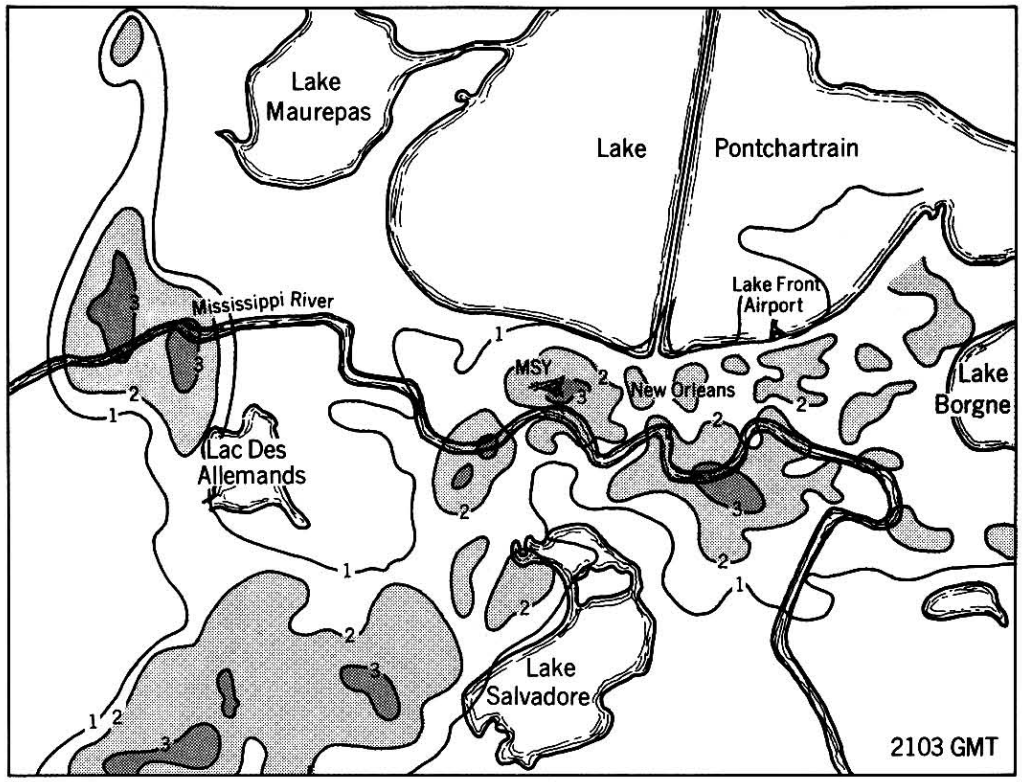

Fig. 4.3 Slidell radar plot for 2103 G M T, 09 July 1982. See Fig. 3.1 caption for details.

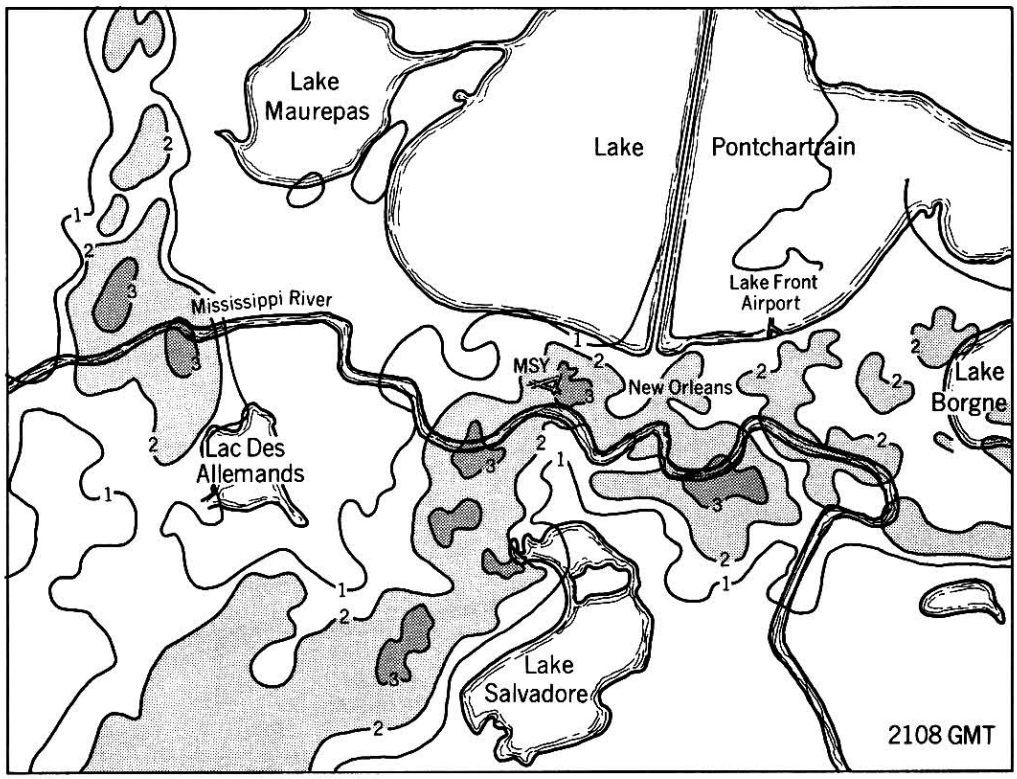

Fig. 4.4 Slidell radar plot for 2108 G M T, 09 July 1982. See Fig. 3.1 caption for details.

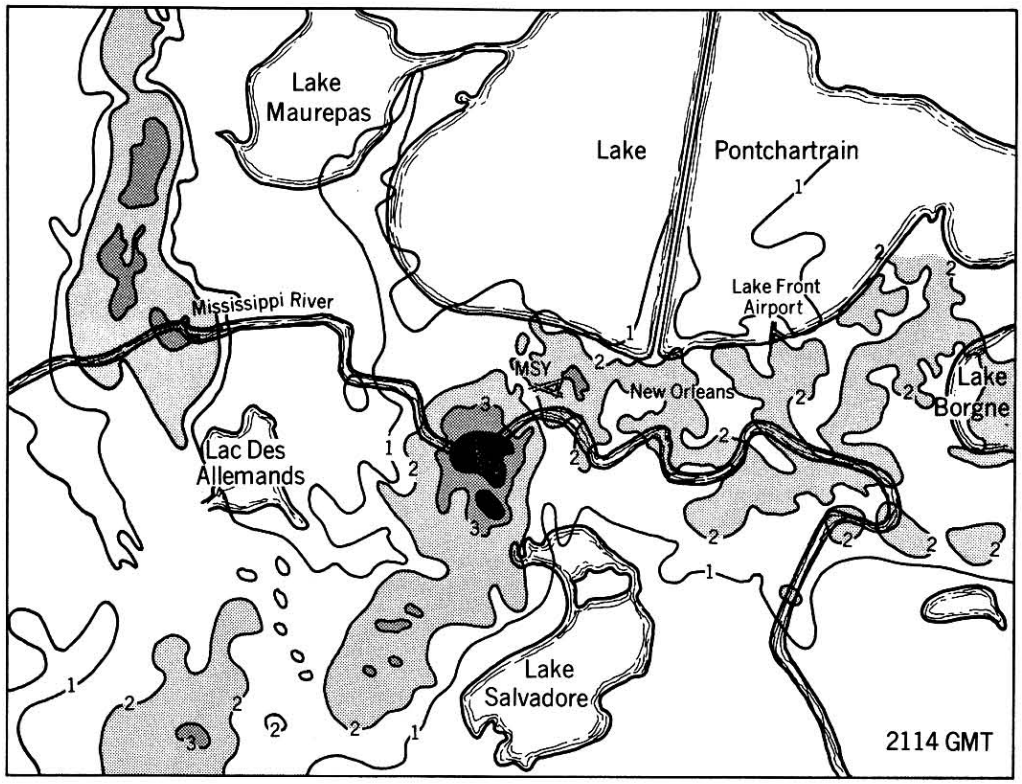

Fig. 4.5 Slidell radar plot for 2114 GMT, 09 July 1982. See Fig. 3.1 caption for details.

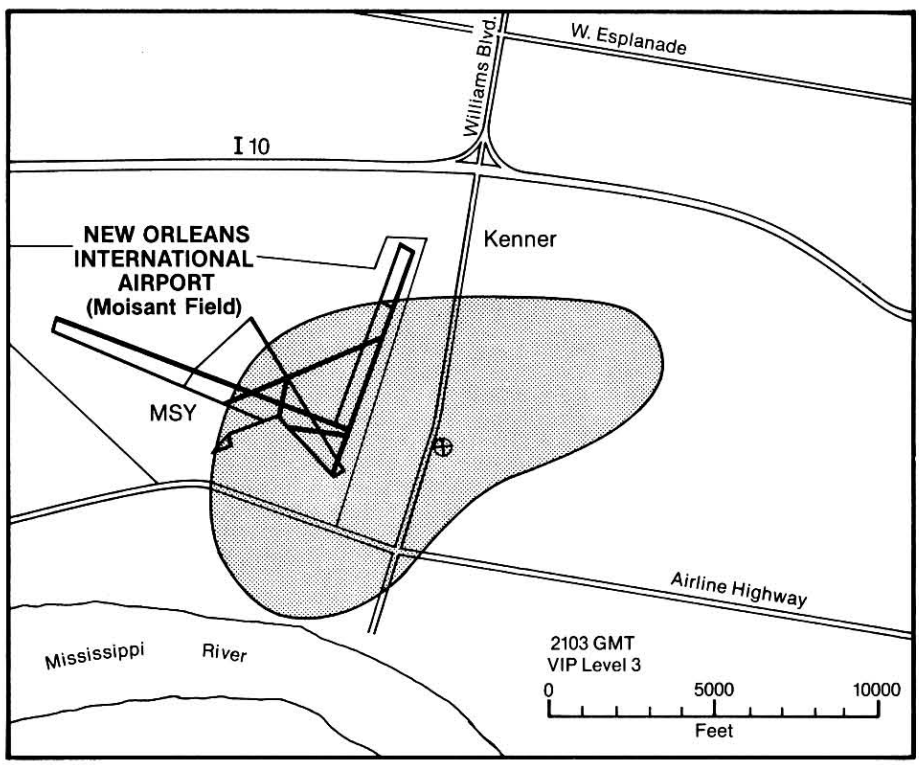

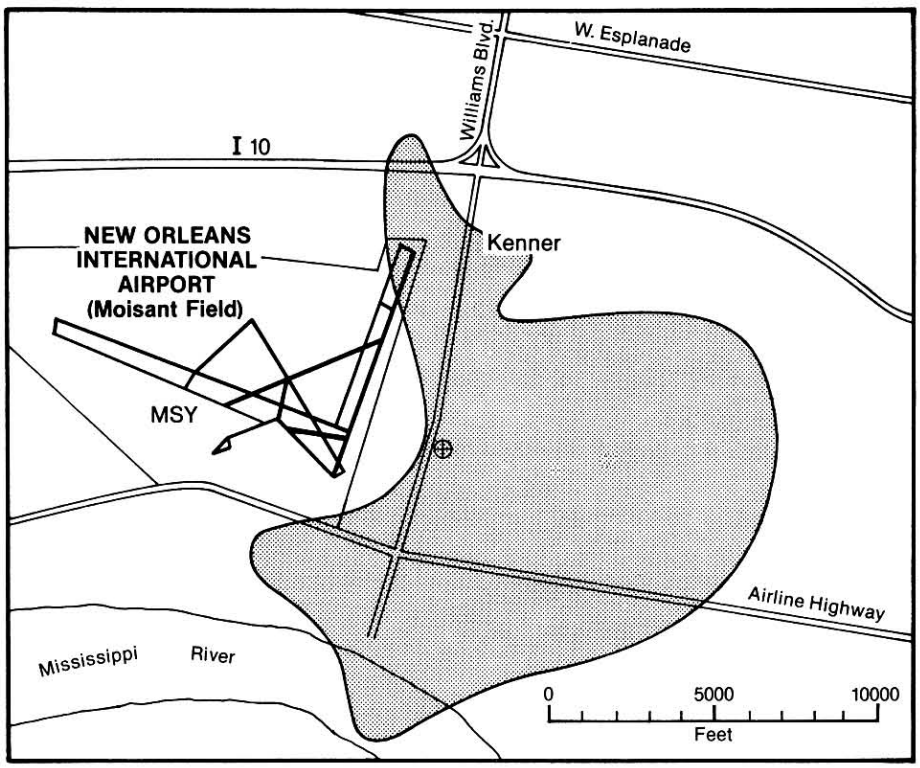

Fig. 4.6 Two Slidell VIP level 3 radar plots showing the shower over MSY at (a) 2103 GMT, 09 July 1982, and five minutes later at (b) 2108 GMT.

area until 2114 (Fig. 4.5) when it dissipated rapidly. By this time the most vigorous echo was a rapidly growing VIP level 4 storm southwest of MSY. After the accident this cell moved northeastward bringing widespread rain to the MSY area.

Despite the satellite analyses discussed in Section 3, the radar appearance of the shower over the departure end of runway 10 at the time of the accident was not remarkable when evaluated according to present operational standards. It presented a small VIP level 3 radar echo that did not exhibit any classic severe thunderstorm signatures. However, from a research point of view it did exhibit two potentially important characteristics.

First, the VIP level 3 portion of the echo was shaped somewhat like a spearhead at 2103 GMT (see Fig. 4.6a). This spearhead shape may be somewhat degraded, relative to the actual cell shape, because the 2^0 wide radar beam was just about equal to the width of the echo. Nevertheless, under similar conditions spearhead echoes have been observed in association with microbursts [see Fujita (1976), Fujita and Beyers (1977), Fujita and Caracena (1977), and Caracena and Meier (1979)].

Second, an arc shaped area of erosion and rapidly weakening echo was seen along the western boundary of the shower at about the time of the accident (see Figs. 4.6a and 4.6b). In fact, a large area of VIP level 3 echo dissipated directly over the path of Pan Am flight 759 between 2103 and 2108 GMT. Fujita (1979) has noted that rapid echo dissipation, which produces notches or arcs, may be associated with the occurrence of microbursts.

4.2 Other Available Data

While the shape and behavior of a poorly resolved radar echo cannot be construed as hard evidence that a microburst occurred, these observations do lend support to the hypothesis that a microburst was involved in the accident. Additional support for this hypothesis is provided by detailed examination of both the aircraft's performance and eyewitness' accounts of the weather.

Pan Am flight 759 apparently suffered a large performance loss just before it crashed. Indeed, after-the-fact reports indicate that this was not an isolated effect and that other aircraft had also experienced problems. About seven minutes before the Pan Am accident, Republic flight 632 had severe difficulties related to very localized weather conditions. Flight 632 departed to the south on runway 19. About one third of way down the runway, the aircraft encountered blinding rain and a strong cross wind from the east. After lift off the stall warning indication activated and continued until the aircraft passed over the departure end of the runway. Just off the departure end of the runway the aircraft experienced an almost instantaneous jump in air speed of about 40 kts, which allowed the Republic crew to recover normal performance. Only 2.5 min. later Texas International flight 794, taking off down the same runway, encountered light to moderate rain and no wind shear. The sudden onset and termination of heavy rain, accompanied by strong and shifting winds, is a characteristic of microbursts.

An analysis of measured winds (note that winds are not recorded within the FAA low-level wind shear network so that readings reported in radio communications were the only information available from this system) and weather conditions reported by eyewitnesses in the immediate vicinity of the airport at the time of the Pan Am accident is shown in Fig. 4.7. A shaft of extremely heavy rain covered the intersection

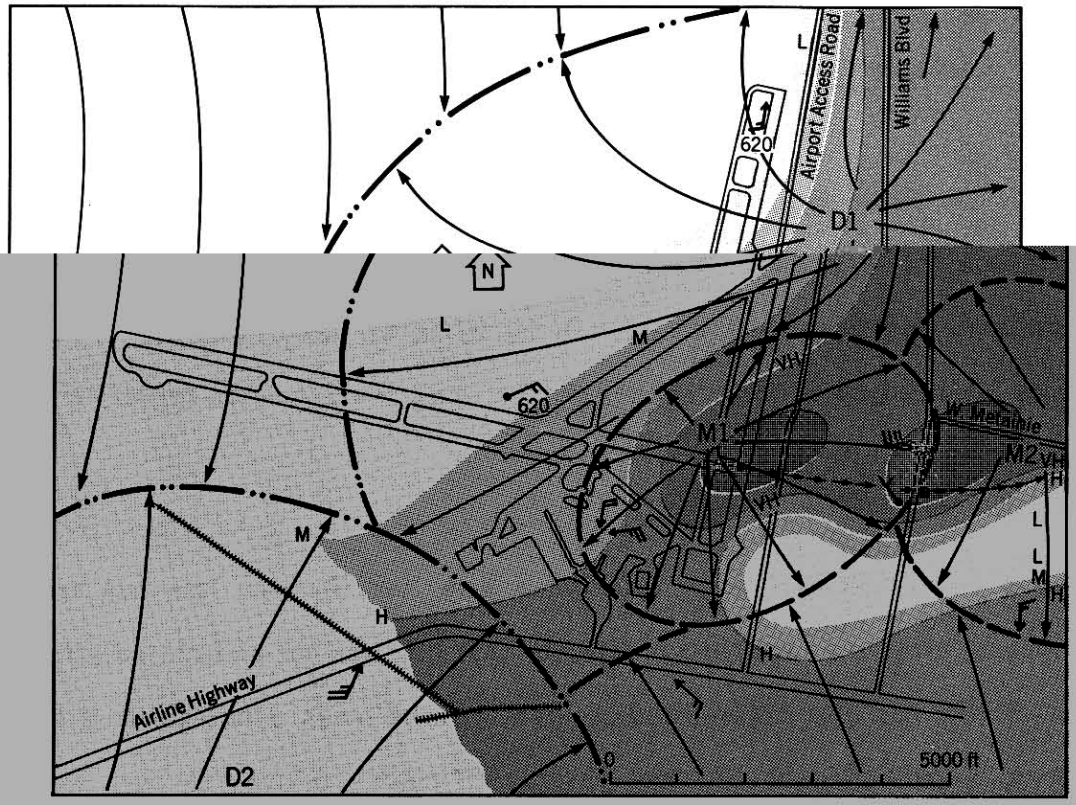

Fig. 4.7 A small scale surface analysis for 2109 GMT, 09 July 1982 based on measured winds and precipitation rates augmented by eyewitness estimates. The rain rates are expressed in a qualitative scale: L=light, M=moderate, H=heavy, VH=very heavy, and EH=extremely heavy. Wind measurements are plotted as normal wind vectors with a full barb representing a speed of 10 kts and a half barb 5 kts. Eyewitness estimates are similarly portrayed except that they are tipped with an arrow.

of runway 19 and 10 at the time of take off. Eyewitnesses along the airport concourses and on the airport access road that parallels runway 19 reported a sudden shift or increase in the wind about the time of take off. The pattern of reported and measured winds indicates that the shaft of heavy rain was an apparent source for strong surface winds that were presumably flowing out in all directions. Flight crews along the concourses saw Pan Am flight 759 taking off and noted a strengthening of the wind from the north-northeast. They felt that the wind was gusting at about 30 kts from the north-northeast. Winds observed on Williams Blvd. may have gusted to as much as 40 kts from the west. Thus, based on these accounts, Pan Am flight 759 faced a potential decrease in head wind component of anywhere from 30 to 60 kts along its takeoff roll.

5. FLIGHT RECORDER DATA

All of the data and information discussed so far suggest that a microburst may have been involved in the crash of Pan Am flight 759. However, detailed analysis of the flight recorder data actually shows that the aircraft did traverse the base of a moderate downdraft in the location where the heavy rain was positioned from eyewitness accounts. (The flight recorder analysis and calculations are discussed in Appendix A.) Results of the analysis, shown in Fig. 5.1, indicate that shortly after lift off the wind shifted from a headwind of about 16 kts to a tailwind of about 23 kts within a distance of about 3400 ft. The inferred vertical velocity along the runway is shown in Fig. 5.2. At the same time that the aircraft crossed the region of adverse headwind gradient it also ascended into the base of a downdraft and encountered a maximum downflow of about 7 ft/s at 100 ft AGL. Linear extrapolation of the vertical wind gradient (assuming zero at the surface) to 300 ft indicates a downdraft of 21 ft/s. This intensity satisfies Fujita's (1976) definition of a downburst (i.e., a localized severe downdraft with a vertical component exceeding 12 ft/s at 300 ft AGL). Further, because of the apparent small

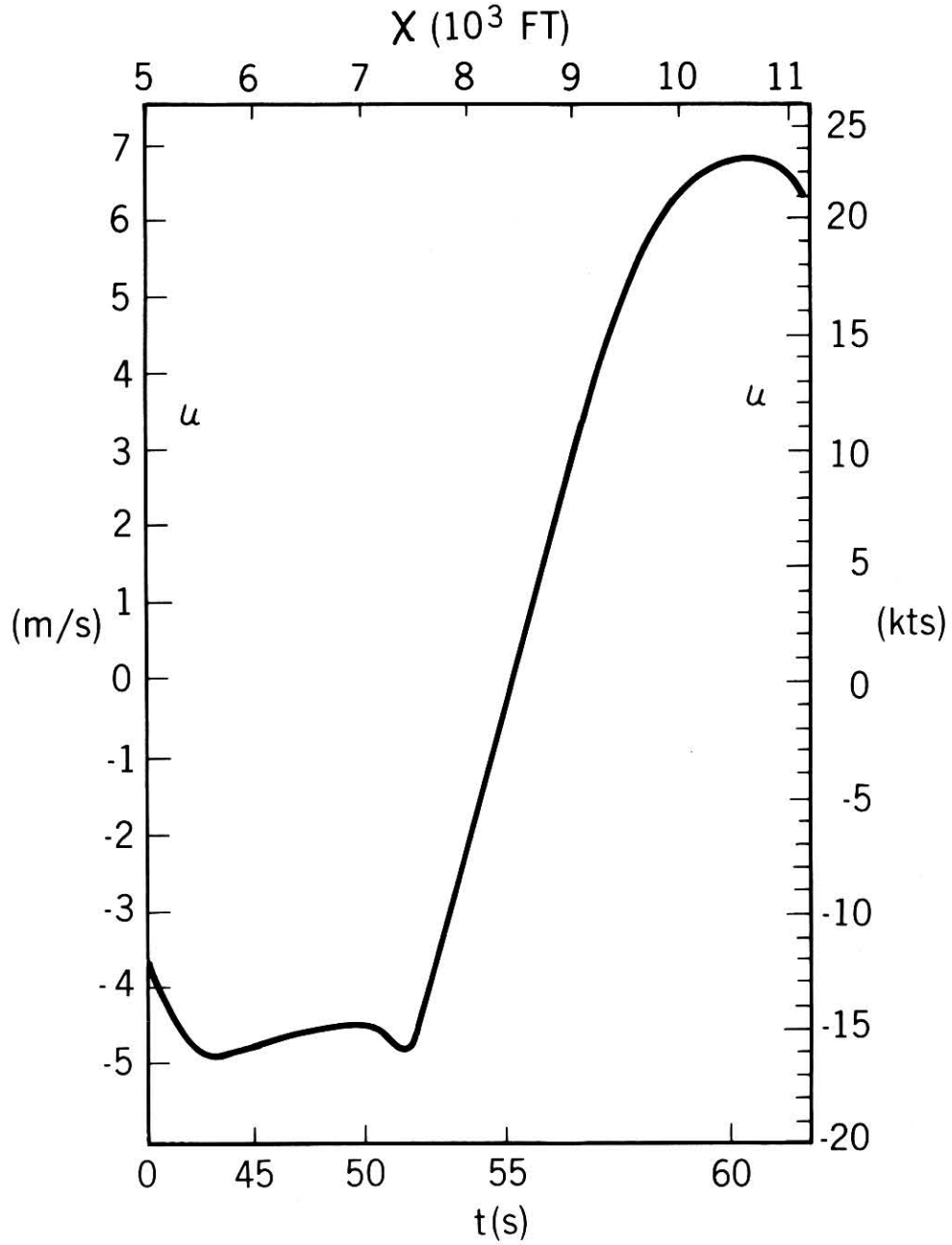

Fig. 5.1 The head/tail wind component encountered by flight 759 determined by integrating the horizontal gradient, $\partial U / \partial X$, in Fig. A.5 with respect to X and using the centerfield measured wind to determine the constant of integration.

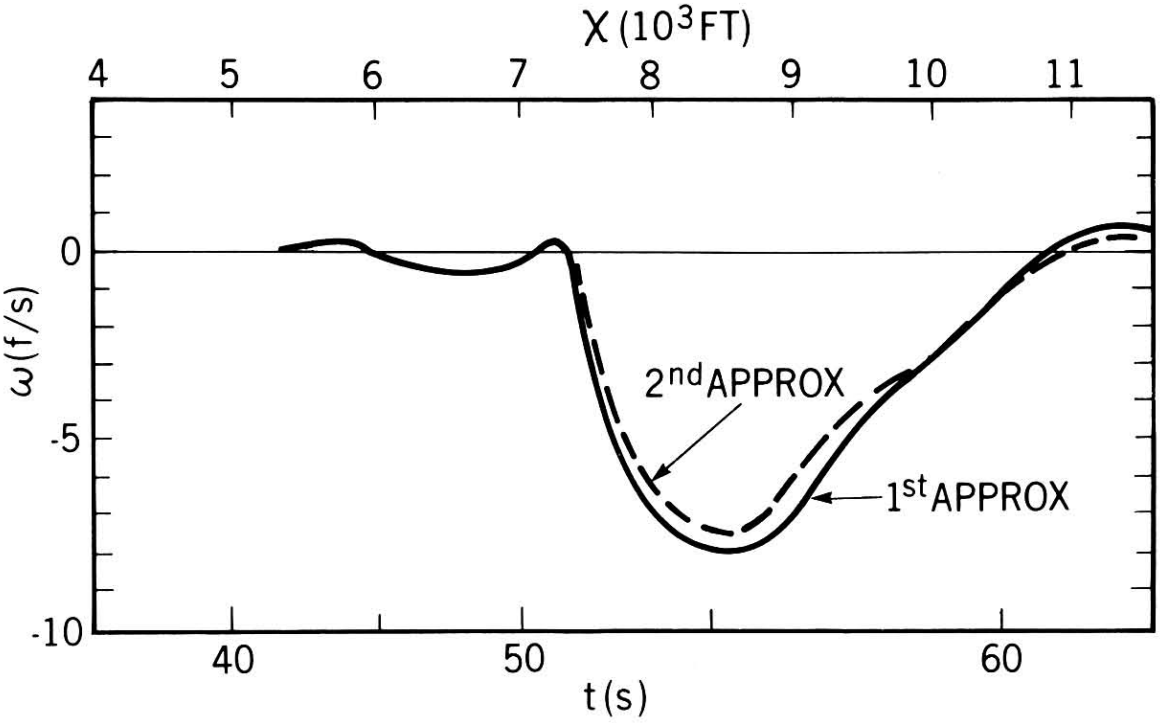

Fig. 5.2 The downdraft component of wind encountered by flight 759 along its flight path in the first approximation (solid curve) and in the second approximation (dashed curve). The small difference indicates that downdraft effects are essentially accounted for in the first approximation.

width of this downburst (<< 4 km) the event also meets Fujita's microburst criteria (i.e., a downburst with its width less than or equal to 4 km). From the data shown here and discussed in detail in Appendix A, it is evident that Pan Am flight 759 experienced downdrafts and horizontal wind shears exhibiting downburst characteristics for about 2000 ft of its flight path.

Luers (1981) has suggested that extremely heavy rainfall rates (>> 100 mm/hour) may have adverse effects on aircraft flight performance. He has further suggested that these effects may be comparable to those associated with severe windshear. However, evaluation of the possible influences of heavy rainfall on Pan Am flight 759 is beyond the scope of this investigation.

6. SUMMARY

Air mass thunderstorms formed in the New Orleans area on the afternoon of July 9th in response to abundant low level moisture and weak synoptic scale forcing mechanisms. A weak upper-air disturbance helped provide the lift that released the convective instability. At low levels, the interaction of several boundaries produced local forcing that initiated and organized the convection. Satellite imagery clearly revealed three intersecting boundaries over MSY. The first of these was a sea breeze front which moved north and was strengthened by downdrafts from thunderstorms that formed along it. The second was a lake breeze front that moved south off of Lake Pontchartrain and had initiated a line of showers extending across MSY to the New Orleans' Lakefront airport. The third was a weak thermal boundary extending from MSY southwestward which was generated by early morning fog and stratus.

In addition, a mass of mid-level dry air developed and approached the region from the north. This air, when cooled by precipitation evaporation, had the potential for generating strong downdrafts. It appears that the air mass storms ingested potentially cold mid-level air in a discontinuous and sporadic manner. This produced localized, intense downdrafts (microbursts) within broader areas of convective rain. Evidence for these conclusions is indirect since none of the microbursts strongly affected a recording meteorological instrument. However, available evidence strongly supports these hypotheses. IR satellite imagery showed that showers over MSY had vigorously growing tops, as evidenced by the rapidly falling cloud top temperatures. The growth rate of these cumulonimbi was much greater than that of any surrounding areas of showers. The rapid growth began several minutes before the crash of Pan Am flight 759 and extended to several minutes afterwards. During this period, two aircraft encounters with low-level windshear occurred.

Slidell radar scope film confirms the existence of a rain shower over Kenner and the east portion of Moisant Field at the time of the accident. Between 2058 and 2108 GMT a VIP level 3 radar echo covered this area. However, by 2114 GMT this echo had weakened and moved northeast as a much larger VIP level 4 echo approached the area from the southwest. The time of the accident corresponded to the period when an arc-shaped portion of the VIP level 3 echo rapidly dissipated directly over the flight path of Pan Am flight 759.

An analysis of wind and precipitation reports, based primarily on eyewitness accounts, reveals that a wide variety of reports did fit a coherent meteorological pattern. The analysis showed that Pan Am flight 759 traversed a localized core of extremely heavy rain at the intersection of runways 10 and 19 and apparently entered another rain-core just before impact. The wind reports also suggest that these rain-cores

were sources of strongly diverging surface winds. In other words, all available meteorological data and eyewitness accounts suggest that Pan Am flight 759 flew through the center of a convectively generated downdraft shortly after lift off. An analysis of the flight recorder data strongly supports the conclusion that this downdraft was a weak to moderate microburst. This analysis shows that Pan Am flight 759 flew through an adverse wind shear of about 39 kts. At the same time it encountered a downdraft of 2000 ft. horizontal extent which meets Fujita's definition of a microburst.

Acknowledgments

We would like to thank Mr. Ken Howard for his help in assembling and plotting data and for helping analyze the radar data. Drs. C.A. Doswell III, J. McCarthy, J. Wilson and C.F. Chappell proof read the manuscript and provided many valuable suggestions. Ms. Jeannie Sanderson skillfully prepared the manuscript.

References

Caracena, F. and M. Maier, (1979): Analysis of a microburst in the FACE meteorological mesonetwork. Preprints, Eleventh Conf. on Severe Local Storms, Kansas City, MO., Amer. Meteorol. Soc., 279-286.

Chandik, J.F. and W. Lyons, (1971): Thunderstorms and the lake breeze front. Preprints, 7th Conf. on Severe Local Storms, Kansas City, MO., Amer. Meteorol. Soc., 218-225.

Fujita, T.T., (1979): Objectives, operation, and results of Project NIMROD. Preprints, Eleventh Conf. on Severe Local Storms, Kansas City, Amer. Meteorol. Soc., 259-266.

Fujita, T.T., (1976): Spearhead echo and downburst near the approach end of a John F. Kennedy Airport runway. New York City. SMRP Res. Paper No. 137, University of Chicago, Ill., 51 pp.

Fujita, T.T. and H.R. Byers, 1977: Spearhead echo and downburst in the crash of an airliner, Mon. Wea. Rev., 105, 129-146.

Fujita, T.T. and F. Caracena, (1977): An analysis of three weather-related aircraft accidents. Bull. Amer. Meteorol. Soc., 58, 1164-1181.

Green, R. and M. Kruidenier, (1982): Interactive data processing for mesoscale forecasting applications. Proc. Ninth Conf. on Weather Forecasting and Analysis, June 28-July 1, Seattle, WA., Amer. Meteorol. Soc., 60-64.

Haurwitz, B., (1947): Comments on the sea breeze circulation. J. Meteor., 4, 1-8.

Luers, J.K., (1981): Effect of heavy rain on aircraft contained in NASA report. CP-2192, pp 76-80. W. Camp and W. Frost, Editors, University of Tennessee Space Inst. 148 pp.

McCarthy, J. and V. Norviel, (1982): Numerical and flight simulator test of the flight deterioration concept. NASA Contractor Report 3500, Washington D.C., 36 pp.

McCarthy, J., E.F. Blick and R.R. Bensch, (1979): Jet transport performance in thunderstorm wind shear conditions. NASA contractor report, 3207, Washington D.C., 61 pp.

Purdom, J.F.W., (1976): Some uses of high-resolution GOES imagery in the mesoscale forecasting of convection and its behavior. Mon. Wea. Rev., 104, 1474-1483.

Turkal, B.S., and W. Frost, (1980): Pilot-Aircraft system response to wind shear. NASA contractor report, 3342. Washington D.C., 106 pp.

Weaver, J.F., (1979): Storm motion as related to boundary-layer convergence. Mon Wea. Rev., 107, 612-619.

APPENDIX A

ANALYSIS OF AIRCRAFT FLIGHT RECORDER DATA

The aircraft flight recorder data were used to estimate the vertical and horizontal components of the wind along the flight track. The method discussed below utilizes only flight recorder data and the recorded wind measurements at the center of the field. Since the aircraft passed within about 100 feet of this instrument we can specify exactly the head/tail wind component at only one point along the aircraft's trajectory. However, we use this as a boundary condition in determining its value over the rest of the aircraft's trajectory. Using a cylindrical model of the downdraft, we employ the equation of continuity to specify the three dimensional wind field for the lower portion of the downdraft.

The method makes use of the following set of equations:

$$U_a = X - U \tag{A.1}$$

where U_a = true airspeed

X = the distance traveled by the aircraft from brake release (approximately along a straight line)

X = the inertial velocity of the aircraft (ground speed)

U = the tail wind component in the direction of aircraft motion (positive for a tail wind).

$$U_a = X - X\, \partial U/\partial X \tag{A.2}$$

$$\partial U/\partial X = (X - U_a)/X \tag{A.3}$$

Equation (A.1) relates the airspeed measured by the aircraft to its relative motion through the air. If the tail wind component, U, vanishes then the indicated airspeed (converted to true airspeed) is identical to the ground speed, X, of the aircraft. The true airspeed is diminished (increased) by an amount equal to the tail (head) wind component. Equation (A.2) is the time derivative of Equation (A.1) taken under the assumption that $\partial U / \partial t = 0$.

Equation A.3 is a solution of A.2 for the horizontal wind shear gradient, $\partial U / \partial X$, in terms of the horizontal acceleration of the aircraft X, its airspeed acceleration U_a, and its horizontal, inertial velocity X. The airspeed acceleration, U_a, is computed directly from the flight recorder values of U_a vs. time. Initially, the aircraft's inertial velocity component, X, can be estimated to within about 10%, in terms of a constant acceleration from brake release to first impact. However the more sensitive horizontal acceleration, X, can be computed with greater precision from the aircraft's vertical component of velocity and the relation:

$$X = (T - D) / M - Z_a (g/U_a). \qquad (A.4)$$

Where the aircraft variables are defined as follows:

T = thrust

Z = height

D = drag

X = inertial acceleration

M = mass

g = acceleration of gravity.

Za = the rate of climb through air.

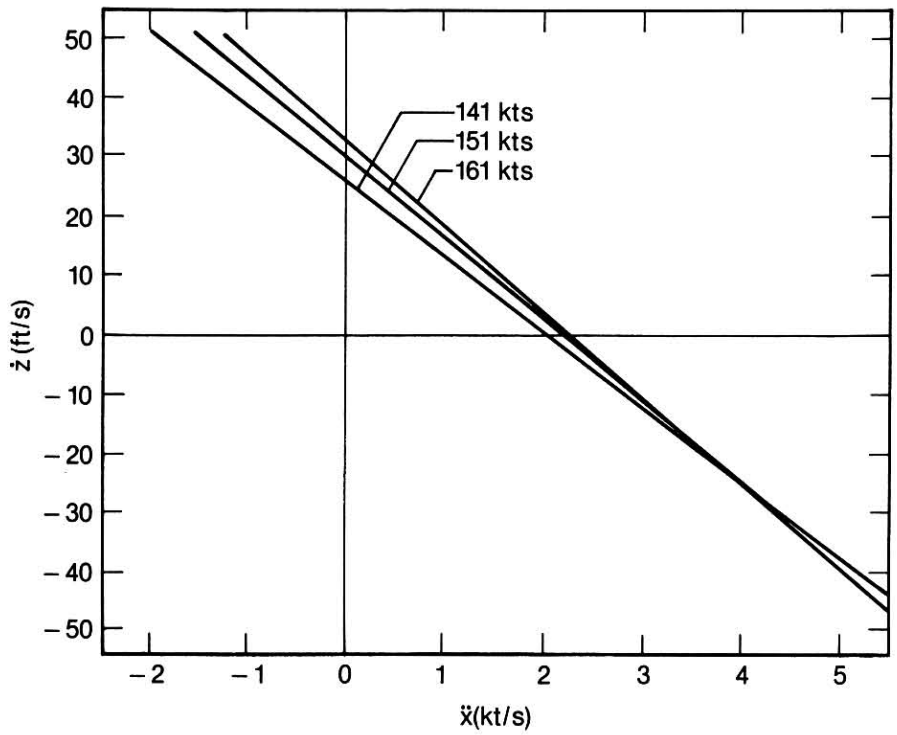

Fig. A.1 Rate of climb vs. horizontal accelerations capability for Pan Am flight 759 from "The aircraft performance analysis" (Docket No SA-479, NTSB Exhibit No 13 J). Each line represents the relation between the rate of climb relative to air vs. the horizontal acceleration for the indicated airspeed.

This relation can be expressed as a family of straight lines relating Z_a to X,

$$X = A(U_a)\, Z_a + B(U_a), \qquad (A.5)$$

where the slopes $A(U_a)$ and intercepts $B(U_a)$ are uniquely determined by the aircraft's airspeed U_a. The data used in determining $A(U_a)$ and $B(U_a)$ for Pan Am flight 759 are from "The aircraft performance analysis" (Docket No. SA-479, Exhibit No. 13 J, NTSB, 1982) which are reproduced in Fig. A.1.

The vertical acceleration data from the flight recorder furnishes the information needed to compute the aircraft's inertial rate of climb, Z. In fact a double integration of the "g - trace" results in a relation of the altitude of the aircraft vs. time which is shown in Fig. A.2. The rate of climb vs. time is depicted in Fig. A.3. This profile is similar to the analytical sine, cosine low-level wind shear models used by McCarthy and Norvill (1982), Turkel and Frost (1980) and McCarthy et al., (1979).

The ground relative rate of climb, Z, can be used as an initial guess in Equation A.5 for the rate of climb through air, Z_a. This means that we initially assume the vertical component of air motion to be zero. With this approximation and Equation A.5 we have computed the horizontal acceleration of the aircraft. The results are displayed in Fig. A.4 as a dashed curve. The airspeed acceleration, U_a, is also displayed in Fig. A.4 as a solid curve. The significant difference that is apparent between X and U_a over a large portion of the airborne trajectory is indicative of strong horizontal windshear (see Equation A.3).

To calculate the horizontal wind gradient, $\partial U/\partial X$, from the data in Fig. A.4 and Equation A.3 some initial guess for X vs. time is required. This was estimated by using the constant horizontal acceleration required to get the aircraft from brake release to first impact in 63 sec. The results of this first approximation are depicted in Fig. A.5

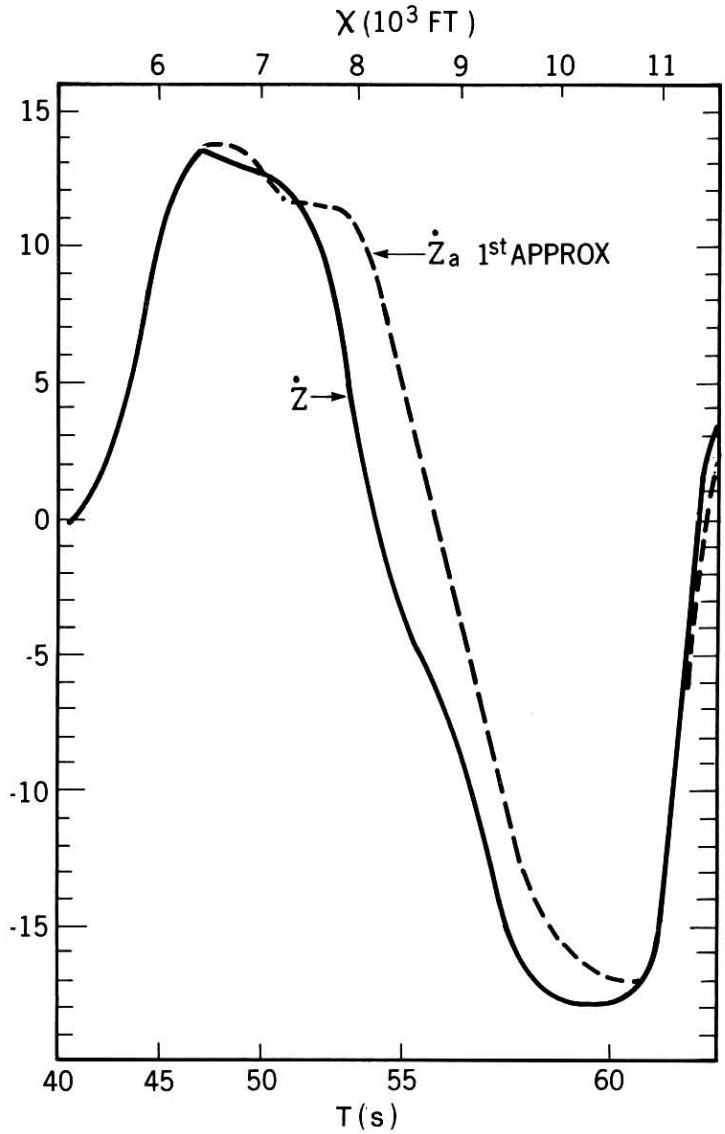

Fig. A.2 The inertial rate of climb (descent) of flight 759 obtained from the first time integration of the vertical acceleration trace (solid curve) from the flight recorder g-trace. The second curve (dashed curve) is the first approximation of the rate of climb of flight 759 relative to air. Note that the time scale is stretched to conform to a linear distance scale.

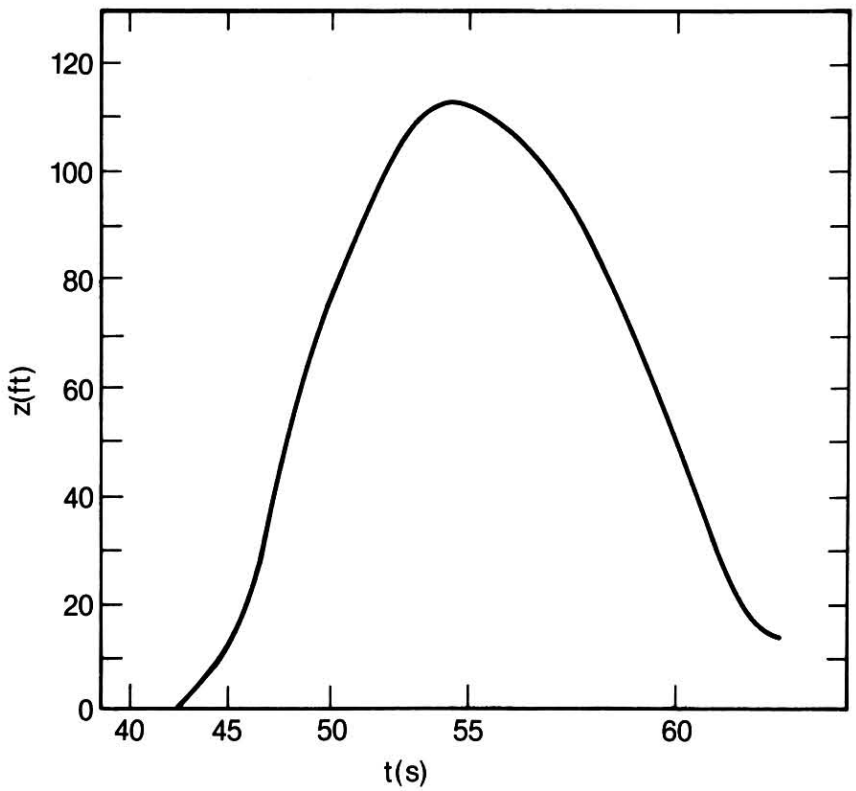

Fig. A.3 The height of flight 759 obtained by integrating the inertial climb rate vs. time in Fig. A.2. A 45 ft error in the initial impact height (260 ft) suggests a systematic error in the vertical acceleration of only 0.2 ft/s^2 and therefore a maximum, accumulated error in the rate of climb in Fig. A.2 of 4.2 ft/s.

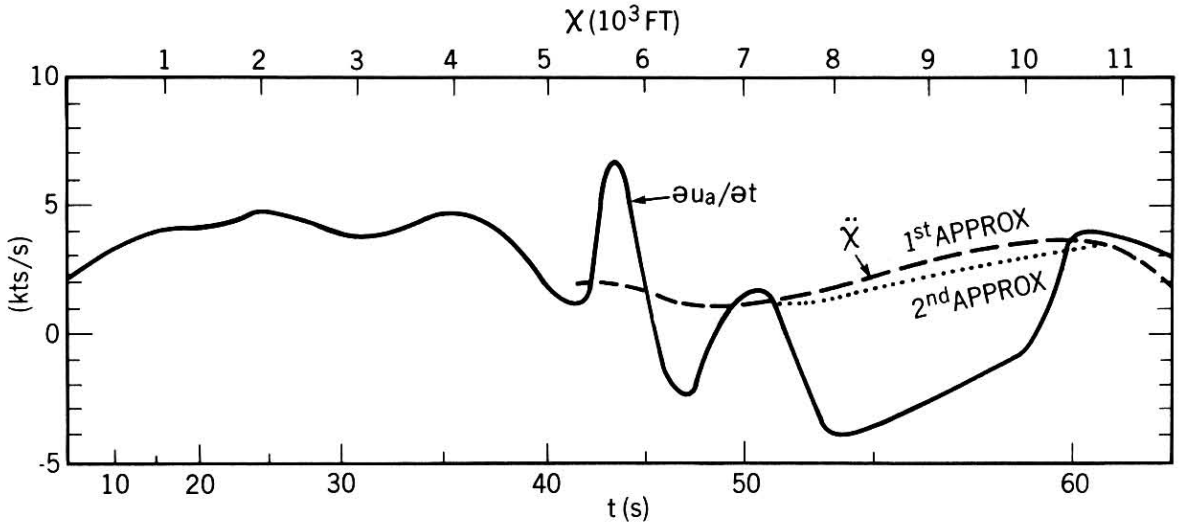

Fig. A.4 The airspeed acceleration of flight 759 vs. time (solid curve, from the flight recorder trace). The inertial acceleration curve (1st approximation, dashed and second approximation, dotted) departs significantly from the airspeed acceleration where flight 759 encountered strong wind shear.

with the dashed portion corresponding to the first approximation of $\partial U/\partial X$ vs. time. These values of $\partial U/\partial X$ serve as data for computing the vertical component of the wind along the aircraft flight path.

Two conditions relate $\partial U/\partial X$ to the vertical wind component. The first is the equation of continuity in an anelastic form,

$$\partial U/\partial X + \partial V/\partial Y + \partial W/\partial Z = 0. \tag{A.6}$$

The second is the assumption of cylindrical symmetry coupled with the assumption that the aircraft made a direct penetration of the microburst (i.e., no cross winds),

$$\partial U/\partial X \simeq \partial V/\partial Y. \tag{A.7}$$

From Equation A.6 and Equation A.7 we then find,

$$\partial W/\partial Z = -2 \partial U/\partial X. \tag{A.8}$$

Further, assuming that the vertical gradient, $\partial W/\partial Z$, is constant with height, we solve for the vertical wind as a function of height,

$$W = -2(\partial U/\partial X) Z. \tag{A.9}$$

Since the vertical component of the aircraft flight trajectory is known (see Fig. A.2) we can solve for the vertical wind component along the flight path. The result is presented in Fig. A.6 (solid curve).

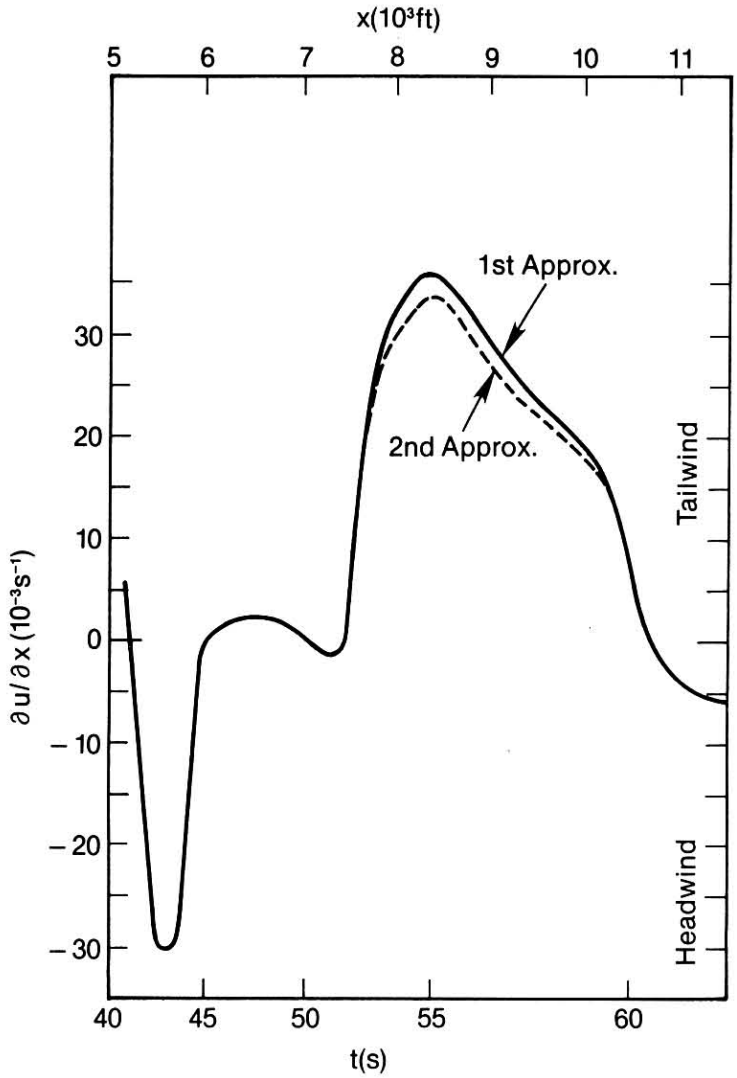

Fig. A.5 The horizontal wind shear gradient (∂ U/ ∂ X) vs. time in the first approximation (solid) with an assumed zero downdraft and in the second approximation (dotted) with the first approximation of the downdraft component.

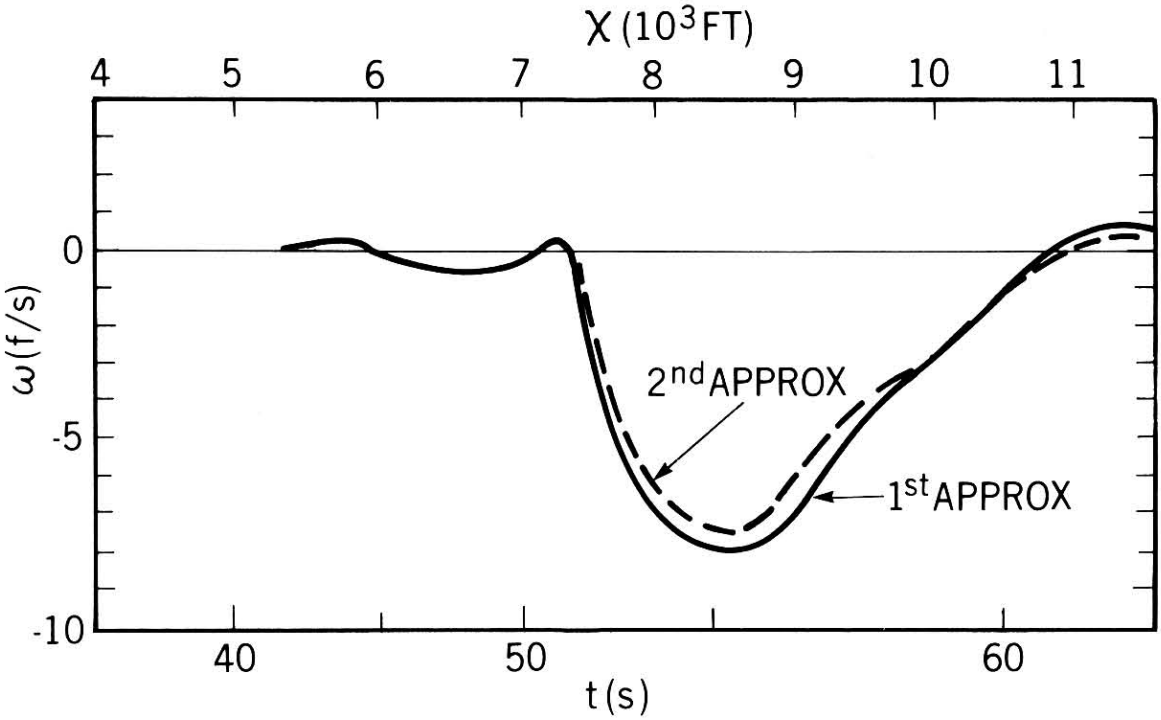

Fig. A.6 The downdraft component of wind encountered by flight 759 along its flight path in the first approximation (solid curve) and in the second approximation (dashed curve). The small difference indicates that downdraft effects are essentially accounted for in the the first approximation.

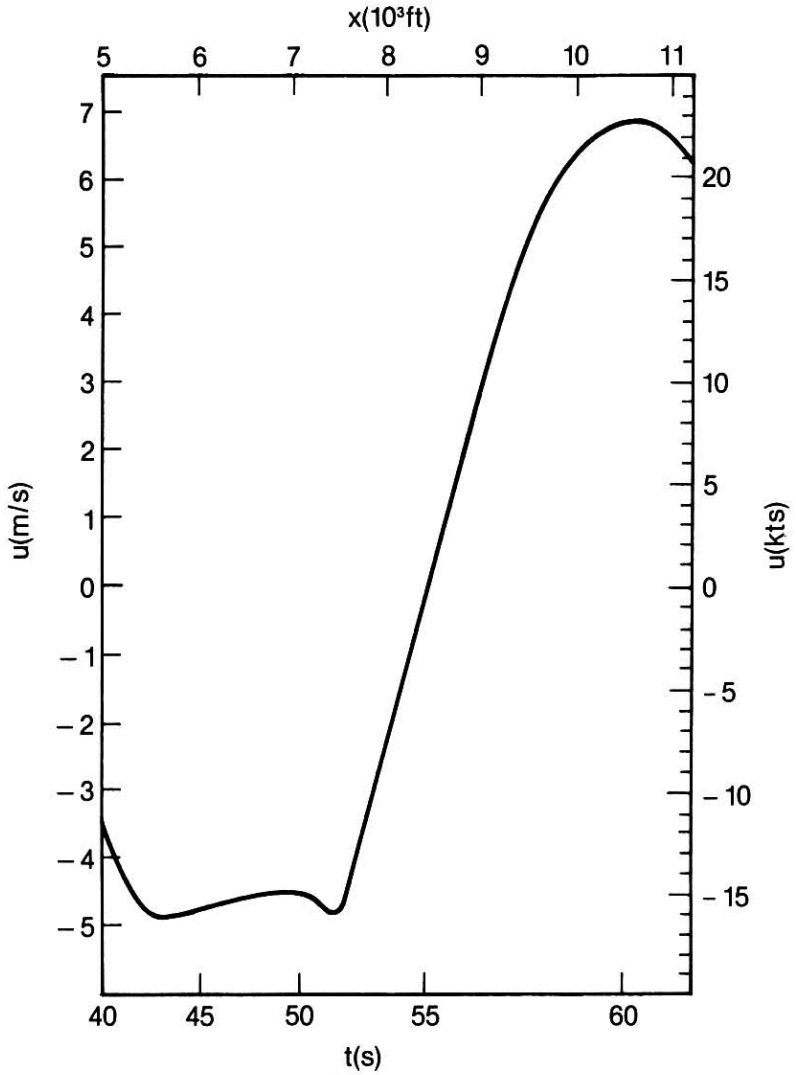

Fig. A.7 The head/tail wind component encountered by flight 759 determined by integrating the horizontal gradient, $\partial U / \partial X$, in Fig. A.5 with respect to X and using the centerfield measured wind to determine the constant of integration.

With knowledge of the vertical component of the wind from Fig. A.6 we can now find the rate of climb of the aircraft through air (see Fig. A.3, dotted curve). Repeating the entire procedure outlined above we arrive at small corrections to the curves in Figs. A.4 - A.6. Notice that this procedure indicates that the second iteration has accounted for most of the vertical wind effects. The error analysis in Fig. A.8 shows that this entire procedure has modified the horizontal velocity profile by 10% or less.

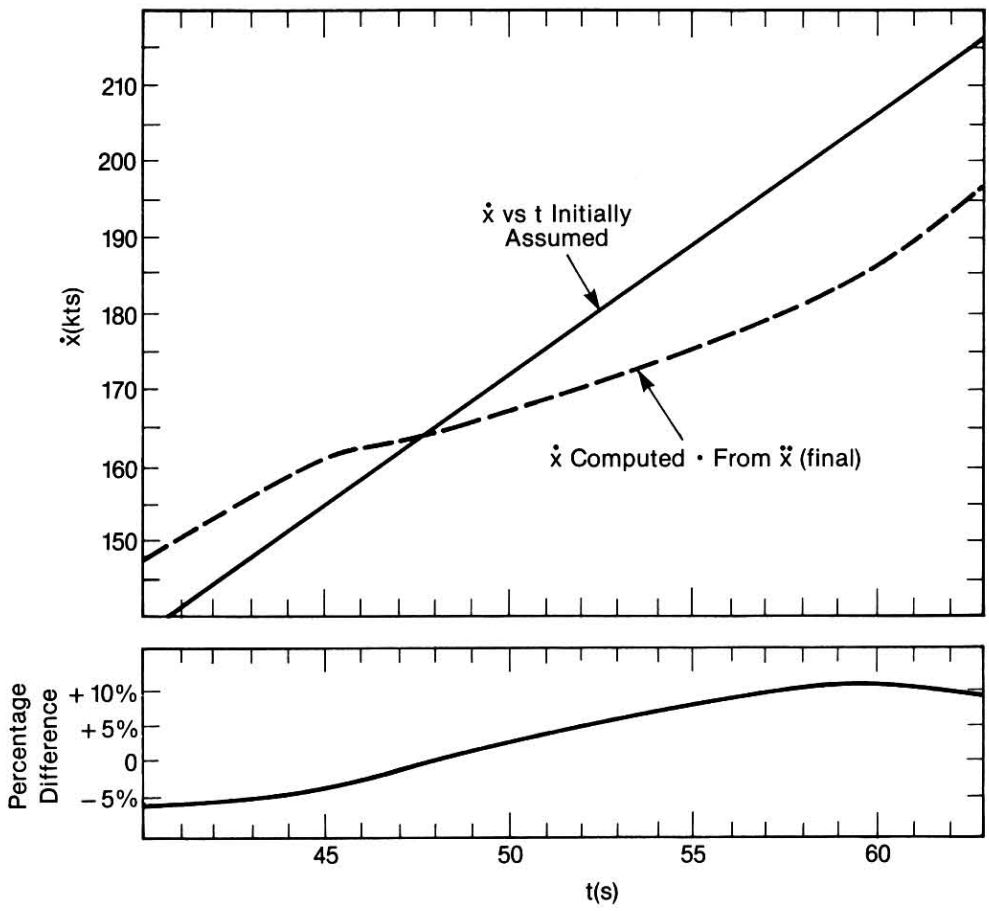

Fig. A.8 Error analysis of the percentage difference between the assumed initial velocity (constant acceleration) and the velocity computed from the horizontal acceleration (second approximation) in Fig. A.4.

APPENDIX B

DEFINITIONS OF COMMON SATELLITE TERMINOLOGY

GEOSYNCHRONOUS - Stationary with respect to a point on earth. A satellite is geosynchronous if its orbital velocity exactly matches the rotation velocity of the earth.

VISSR - A satellite radiation sensor which constructs pictures at visual (VIS) and thermal infrared (IR) wavelengths. VIS pictures are simply black and white cloud photos. IR pictures are photos of cloud top temperatures which can be related, in turn, to cloud top height. The VISSR unit spins about its own axis at ~ 100 rpm. as it hovers in orbit. The spin acts to stabilize the sensor's pitch and roll.

Due to data resolution and transmission requirements, VISSR pictures are constructed from a series of hundreds of individual horizontal lines (as in television pictures). One photo line is taken on each revolution, the sensor then changes its viewing direction by a slight angle, and the next line is scanned. Thus, the acronym VISSR--Visual and Infrared Spin Scan Radiometer.

GOES - Geosynchronous Operational Environmental Satellite GOES satellites are VISSR units which utilize a 16-inch aperature telescope for scanning. There are normally two GOES units in operations at any one time; GOES-East hovering at 0^{o} N/75^{o} W and GOES - West at 0^{o} N/135^{o} W.

RRSD - Research Rapid Scan Day. Days on which the normal half hour interval, 1831 scanline, full globe schedule is replace by a 3 minute interval, 275 scanline, limited-area schedule for scientific research purposes. The more frequent photographs allow better understanding of rapidly changing weather patterns. However, it should be noted that the amount of data collected on RRSDs is massive and cannot be processed in real time. Thus, such data are used for research purposes only.

PIXEL - PIctures ELement, representing the unit of data transmitted or the resolution of the satellite product. Both the north-south and east-west resoultion are limited to the amount of information that can be transmitted and processed by the system. The size of a VIS Pixel is 0. 5 X 0.5 miles at the equator, while an IR Pixel is 0.4 X 2.0 miles at the equator. Pixel size is slightly greater at higher latitudes, owing to changing camera angle.